



HAL
open science

PROSPECT-PRO for estimating content of nitrogen-containing leaf proteins and other carbon-based constituents

Jean-Baptiste Féret, Katja Berger, Florian de Boissieu, Zbyněk Malenovský

► To cite this version:

Jean-Baptiste Féret, Katja Berger, Florian de Boissieu, Zbyněk Malenovský. PROSPECT-PRO for estimating content of nitrogen-containing leaf proteins and other carbon-based constituents. Remote Sensing of Environment, 2021, 252, pp.112173. 10.1016/j.rse.2020.112173 . hal-03009580

HAL Id: hal-03009580

<https://hal.inrae.fr/hal-03009580v1>

Submitted on 17 Nov 2020

HAL is a multi-disciplinary open access archive for the deposit and dissemination of scientific research documents, whether they are published or not. The documents may come from teaching and research institutions in France or abroad, or from public or private research centers.

L'archive ouverte pluridisciplinaire **HAL**, est destinée au dépôt et à la diffusion de documents scientifiques de niveau recherche, publiés ou non, émanant des établissements d'enseignement et de recherche français ou étrangers, des laboratoires publics ou privés.

14 **Abstract**

15 Models of radiative transfer (RT) are important tools for remote sensing of vegetation, allowing for
16 forward simulations of remotely sensed data as well as inverse estimation of biophysical and biochemical
17 traits from vegetation optical properties. Estimation of foliar protein content is the key to monitor the
18 nitrogen cycle in terrestrial ecosystems, in particular to assess the photosynthetic capacity of plants and
19 to improve nitrogen management in agriculture. However, until now physically based leaf RT models have
20 not allowed for proper spectral decomposition and estimation of leaf dry matter as nitrogen-based
21 proteins and other carbon-based constituents (*CBC*) from optical properties of fresh and dry foliage. Such
22 an achievement is the key for subsequent upscaling to canopy level and for development of new Earth
23 observation applications.

24 Therefore, we developed a new version of the PROSPECT model, named PROSPECT-PRO, which separates
25 the nitrogen-based constituents (proteins) from *CBC* (including cellulose, lignin, hemicellulose, starch and
26 sugars). PROSPECT-PRO was calibrated and validated on subsets of the LOPEX dataset, accounting for both
27 fresh and dry broadleaf and grass samples. We applied an iterative model inversion optimization
28 algorithm and identified the optimal spectral ranges for retrieval of proteins and *CBC*. When combining
29 leaf reflectance and transmittance within the selected optimal spectral domains, PROSPECT-PRO
30 inversions revealed similarly accurate *CBC* estimates of fresh and dry leaf samples (respective validation
31 $R^2 = 0.96$ and 0.95 , $NRMSE = 9.6\%$ and 13.4%), whereas a better performance was obtained for fresh than
32 for dry leaves when estimating proteins (respective validation $R^2 = 0.79$ and 0.57 , $NRMSE = 15.1\%$ and
33 26.1%). The accurate estimation of leaf constituents for fresh samples is attributed to the optimal spectral
34 feature selection procedure.

35 We further tested the ability of PROSPECT-PRO to estimate leaf mass per area (*LMA*) as the sum of
36 proteins and *CBC* using independent datasets acquired for numerous plant species. Results showed that
37 both PROSPECT-PRO and PROSPECT-D inversions were able to produce comparable *LMA* estimates across

38 an independent dataset gathering 1685 leaf samples (validation $R^2 = 0.90$ and $NRMSE = 16.5\%$ for
39 PROSPECT-PRO, and $R^2 = 0.90$ and $NRMSE = 18.3\%$ for PROSPECT-D). Findings also revealed that
40 PROSPECT-PRO is capable of assessing the carbon-to-nitrogen ratio based on the retrieved *CBC*-to-
41 proteins ratio ($R^2 = 0.87$ and $NRMSE = 15.7\%$ for fresh leaves, and $R^2 = 0.65$ and $NRMSE = 28.1\%$ for dry
42 leaves). The performance assessment of newly designed PROSPECT-PRO demonstrates a promising
43 potential for its involvement in precision agriculture and ecological applications aiming at estimation of
44 leaf carbon and nitrogen contents from observations of current and forthcoming airborne and satellite
45 imaging spectroscopy sensors.

46

47 1. INTRODUCTION

48 Nitrogen (N) is a major nutrient for all living plant organisms, cultivated as well as wild forms. In
49 agriculture, crop yield quality is primarily dependent on protein content, with the N availability being the
50 most critical factor of actual grain protein content (Brown et al., 2005). N limitation in soil and plants
51 generally restricts the development and growth of roots, suppresses lateral root initiation, increases the
52 carbon-to-nitrogen (C:N) ratio within the plant, reduces photosynthesis, and results in early leaf
53 senescence (Kant et al., 2011; Paul and Driscoll, 1997; Wingler et al., 2006). On the other hand, N over-
54 fertilization is undesirable for quality of both crops and environment. Excess of N reduces yield and
55 decreases its quality (e.g., organoleptic quality), reduces the content of mineral nutrients and secondary
56 metabolites, and increases nitrate content in leaves (Albornoz, 2016). From the environmental
57 perspective, the human activity that altered the global N cycle by through N fertilization of farming
58 systems has negative impacts on terrestrial and aquatic ecosystems (Davidson et al., 2011; Gruber and
59 Galloway, 2008). The consequences include habitat eutrophication, acidification, and contribution to the
60 accelerated loss of biodiversity caused by decreased competitive advantage of plants adapted to efficient
61 use of nitrogen (Vitousek et al., 1997). Optimization of N management has, therefore, an important role

62 in mitigating such effects, while securing sufficient and sustainable food production. N concentration in
63 plants is, in general, considered as an important surrogate measure for plant photosynthetic capacity
64 (Evans, 1989), and its remote estimation is, therefore, of a great interest for plant biology and ecology.
65 Remotely sensed (RS) monitoring of N in vegetation is a prospective tool for N management improvement
66 and for reduction of negative impacts imposed by conventional farming. Decision support systems that
67 use RS information are mostly based on the relationship between leaf N and chlorophyll content. Such
68 monitoring has certain operational advantages, originating from strong chlorophyll *a+b* spectral
69 absorption features in the visible domain, but also from a great diversity of physically based, data driven
70 and hybrid methods designed to estimate chlorophylls from multi- and hyperspectral data (Baret et al.,
71 2007; Clevers and Gitelson, 2013; Malenovský et al., 2013; Verrelst et al., 2015). Although a significant
72 amount of literature reported a strong correlation between leaf N and chlorophyll content in crops (Baret
73 et al., 2007; Clevers and Kooistra, 2012; Vos and Bom, 1993; Yoder and Pettigrew-Crosby, 1995), this
74 relationship does not hold during their senescence and does not appear to be universal, as it is relatively
75 weak across species and ecosystems (Asner and Martin, 2009; Homolová et al., 2013). N is involved in
76 many leaf physiological processes, including photosynthesis, respiration, structural growth and storage
77 capacity building (Liu et al., 2018). This results in multiple N-based leaf biochemical constituents with
78 different physiological roles that are created throughout the plant life cycle in response to changing
79 environmental factors. Chlorophyll pigments contain only a small fraction of N, representing less than 2%
80 of the total leaf N (Kokaly et al., 2009). In comparison, proteins are the major nitrogen-containing
81 biochemical constituents, with Ribulose-1,5-bisphosphate carboxylase/oxygenase (rubisco enzyme)
82 holding 30–50% of N that is present in green leaves (Elvidge, 1990; Kokaly et al., 2009). Rubisco, the most
83 abundant protein on Earth, catalyzes the photosynthetic fixation of carbon dioxide (Sharwood, 2017).
84 Together with other photosynthesis-related proteins, it is the major source of N available for
85 remobilization among plant parts (Masclaux-Daubresse et al., 2010). For instance, N in oilseed rape

86 (*Brassica napus*) remobilizes from senescing to expanding leaves during the vegetative growth stage and
87 from senescing leaves to seeds during the reproductive stage (Malagoli, 2005). This indicates that, unlike
88 chlorophyll, plant nitrogen content does not decrease upon reaching mature growth stages, but is rather
89 translocated to other organs, which makes the relationship between plant nitrogen and leaf chlorophyll
90 content through the vegetation growth cycle nonlinear. Consequently, a quantitative non-destructive
91 retrieval of leaf protein content is expected to be a more reliable proxy of nitrogen content (Berger et al.,
92 2020b).

93 As reported in the pioneering studies from Curran (1989), Elvidge (1990) and Himmelsbach et al. (1988),
94 the absorption features corresponding to proteins are caused mainly by N-H bond stretches. They are
95 located in the shortwave infrared (SWIR) domain between 1500 and 2400 nm, with two additional
96 features reported in the near infrared (NIR) domain at 910 and 1020 nm. The quantification of proteins
97 from leaf optical properties is, however, challenging, because of their relatively low concentrations, and
98 some of their specific absorption features being overlapped by absorption features from water or other
99 dry matter constituents (Fourty et al., 1996; Jacquemoud et al., 1996). At the canopy scale, additional
100 confounding factors (e.g., vegetation structure, geometry of acquisition or soil and atmosphere
101 properties, etc.) also contribute to the reflectance signal measured by optical sensors. Multispectral
102 systems with broad spectral bands and moderate spectral sampling are insufficient to correctly
103 differentiate biochemical constituents with narrow and overlapping absorption features. The contiguous
104 narrow spectral bands measured with imaging spectroscopy are more suitable to differentiate spectral
105 features corresponding to the combination of multiple optically active constituents (Hank et al., 2019).
106 Even subtle contributions of proteins to the hyperspectral signal may allow their accurate estimation, if
107 using appropriate methods. Such methods include multivariate statistical and machine learning
108 algorithms, physically based approaches or hybrid combinations of both (Verrelst et al., 2019a).

109 Physical models offer a certain number of advantages over empirical and machine learning approaches.
110 The physically explicit representation of the interactions between electromagnetic radiation and
111 vegetation structures enables forward simulation and inversion of reflectance signals acquired by any
112 laboratory/field, close-range, airborne or space-borne spectroradiometer. Their main advantages, when
113 compared to empirical methods, are robustness and transferability, although recent publications suggest
114 that these advantages may not be as large as expected (Serbin et al., 2019). The definition of a physical
115 model that includes proteins as an input requires the calibration of specific absorption coefficients for
116 proteins and other constituents of dry matter in leaves, which has proven to be challenging (Botha et al.,
117 2006; Kokaly et al., 2009). Jacquemoud et al. (1996) developed a version of the PROSPECT model including
118 specific absorption coefficients for proteins and for different combinations of carbon-based constituents
119 (*CBC*), but the model inversion resulted in moderate to good estimates of proteins (R^2 between 0.49 and
120 0.67) and different combinations of *CBC* (R^2 between 0.39 and 0.88) in dry leaves and poor to moderate
121 accuracy for proteins ($R^2 < 0.05$) and *CBC* ($R^2 < 0.50$) in fresh leaves. Wang et al. (2015) updated a later
122 version of PROSPECT to include proteins and lignin plus cellulose. They concluded on the importance of
123 selecting specific spectral domains to obtain optimal results, which was later confirmed by Féret et al.
124 (2019) when inverting PROSPECT for estimation of leaf dry mass per area (*LMA*) and equivalent water
125 thickness (*EWT*). However, both Jacquemoud et al. (1996) and Wang et al. (2015) assumed that only
126 proteins, lignin and cellulose, representing about 75% of *LMA*, contribute to leaf absorption. They
127 excluded spectral contribution of non-structural carbohydrates (e.g., sugars and starch), which is a
128 significant source of forward and inverse modelling uncertainties.

129 Our overall objective is to develop a new version of the PROSPECT model capable of differentiating and
130 accurately estimating protein and *CBC* contents from leaf spectroscopic measurements. The new
131 PROSPECT version, named PROSPECT-PRO, should be applicable to all types of bifacial leaves, including
132 fresh green as well as senescent and dry leaves. As a secondary objective, we intend to identify optimal

133 spectral domains for quantitative estimation of leaf proteins through a PROSPECT-PRO inversion and
134 validate its performance on independent datasets of leaf optical and biochemical measurements. The
135 introduced improvements in PROSPECT-PRO leverage only shortwave infrared (SWIR, 1000-2500 nm)
136 wavelengths, where protein and *CBC* absorption features are prominent, and therefore does not affect
137 the existing functionality of PROSPECT with respect to foliar pigments.

138 We provide a general introduction to the PROSPECT model physical principles in Section 2. The data used
139 for the calibration and validation of PROSPECT-PRO are described in Section 3. Explanation of the
140 calibration procedure, including analytical tools for global sensitivity analysis, validation and identification
141 of optimal retrieval spectral domains, is given in Section 4. Section 5 presents the results of the study.
142 Finally, Section 0 discusses potential applications of and limitations to PROSPECT-PRO, are concluding
143 findings are presented in Section 7.

144

145 2. General introduction of PROSPECT

146 PROSPECT is a physical model simulating leaf directional-hemispherical reflectance and transmittance
147 (Schaepman-Strub et al., 2006) using a relatively low number of biophysical and biochemical input
148 parameters. Its first version was developed by Jacquemoud and Baret (1990) as an extension of the
149 generalized plate model of Allen et al. (1970, 1969), with later versions developed to include more
150 absorbing constituents (Jacquemoud et al., 1996; Féret et al., 2008, 2017) or to adapt to specific
151 conditions and leaf types, for example needle-shaped leaves (Malenovský et al., 2006). The PROSPECT
152 model was also the starting point for development of independent extensions modelling RT of leaf
153 chlorophyll fluorescence, such as FluorMODleaf (Pedrós et al., 2010) and Fluspect (van der Tol et al., 2019;
154 Vilfan et al., 2018). PROSPECT can be used in forward mode to simulate leaf optical properties from the
155 description of its biochemical and structural properties, or in inverse mode to estimate part or all of these

156 biochemical and structural properties based on measured leaf optical properties. Detailed description of
157 these modes is provided in Section 4.

158 In addition to the leaf biochemical variables such as foliar pigments, *EWT* and *LMA*, PROSPECT requires a
159 unique leaf mesophyll structure parameter N_{struct} . In a simplified leaf representation, described by the
160 generalized plate model, it corresponds to the number of uniform compact plates separated by $N_{struct} -$
161 1 air spaces. N_{struct} describes the complexity of a leaf internal structure, where a low value (1-1.5)
162 indicates a simpler compact mesophyll tissue (e.g., monocots) while a high value (1.5-2) indicates
163 mesophyll of a greater complexity containing more intercellular air spaces (e.g., eudicots) (Boren et al.,
164 2019). N_{struct} governs leaf internal light scattering, but it has a negligible impact on leaf absorption.
165 Higher values of N_{struct} result in a greater reflectance and a decreased transmittance, which is obvious
166 primarily in spectral domains of low absorption (e.g., NIR wavelengths). To date, N_{struct} is estimated
167 indirectly from NIR leaf reflectance and transmittance measurements (Féret et al., 2019). Since we used
168 the most recent model version PROSPECT-D as the basis for establishing a new PROSPECT-PRO, the
169 wavelength dependent refractive index of leaf interior and the specific absorption coefficients for water
170 remained identical to PROSPECT-D.

171

172 3. MATERIAL

173 a. Calibration and validation data to establish PROSPECT-PRO

174 The calibration and validation datasets must include directional-hemispherical leaf reflectance and
175 transmittance and corresponding biochemical destructive measurements of the constituents used as
176 model inputs, but only constituents with optical activity within the spectral range in which calibration is
177 performed are needed. Since the new additions in PROSPECT-PRO utilize only the SWIR domain covering
178 protein absorption features, contents of foliar pigments were not required for its calibration. The Leaf
179 Optical Properties Experiment (LOPEX) dataset, established by the Joint Research Center (JRC) of the

180 European Commission (Ispra, Italy) in 1993 (Hosgood et al., 1994), contains optical, physical and
181 biochemical measurements of more than 50 plant species collected around Ispra, Italy. Although this
182 species diversity guarantees a certain variability in leaf optical and biochemical properties, the data used
183 for the calibration of PROSPECT-PRO certainly does not cover the full range of variability across existing
184 biomes. On the other hand, this dataset has, based on our search, the only publicly available data suitable
185 for this calibration. We acknowledge that additional datasets obtained from various ecosystem types and
186 growing conditions are required for a future PROSPECT-PRO verification. The optical properties of leaf
187 directional-hemispherical reflectance and transmittance were measured with an integrating sphere from
188 the visible (VIS) to shortwave infrared region (VSWIR, 400-2500 nm). The biochemical measurements of
189 photosynthetic pigments, water (*EWT*) and generic dry matter (*LMA*) content, as well as carbon (C),
190 hydrogen, oxygen, nitrogen, lignin, proteins, cellulose and starch content are expressed as a percentage
191 of dry mass. The protein content in the original LOPEX dataset was estimated from the nitrogen content
192 measured by the Kjeldahl method (Bradstreet, 1954; Sáez-Plaza et al., 2013) using the nitrogen-to-crude
193 protein conversion factor of 6.25, which is widely used for food materials. We used the revised factor of
194 4.43, as suggested by Yeoh and Wee (1994) to be more representative of a broader range of vegetation
195 types. This transformation of the protein content is one of the functional differences between our model
196 and models calibrated in previous studies (Fourty et al., 1996; Jacquemoud et al., 1996; Wang et al., 2015).
197 As the original version of LOPEX includes 120 samples, encompassing broad leaves, needles, stalks, and
198 powders, we used only data corresponding to bifacial monocotyledon and eudicotyledon leaves. The five
199 reflectance and transmittance measurements taken for each sample were averaged. For some samples,
200 the measurements of optical properties were taken from both fresh and dry leaves. Therefore, we
201 separated these measurements and produced two distinct datasets of dry and fresh samples. Chemical
202 measurements were performed by two independent laboratories in Belgium and France (Verdebout et
203 al., 1995). Although measurements of both laboratories were relatively consistent, we decided to use the

204 chemical analyses from the Belgian laboratory, leading to slightly improved overall results during
205 calibration and validation stages. The chemical compositions measured several times over the same
206 samples to test repeatability of lab measurement protocols were averaged. One sample of alder (*Alnus*
207 *glutinosa*) with a particularly low SWIR transmittance (less than 1% on average between 1900 and 2500
208 nm and across spectral domains with less than 0.1% of transmittance) was discarded from the fresh
209 samples, because its presence systematically prevented a proper calibration and validation across all tests
210 of the data. Additionally, two fresh samples of beech (*Fagus sylvatica L.*) and poplar (*Populus canadensis*)
211 leaves were placed in the validation data, because their presence in the calibration data resulted in
212 systematically poor results. These three samples were all characterized by a high *EWT* > 0.030 cm (i.e. 30
213 mg.cm⁻²). The final selection of the LOPEX dataset resulted in 66 fresh and 49 dry eligible samples.
214 To our best knowledge, LOPEX is the only open dataset that includes required information on leaf protein
215 content for the calibration and validation of PROSPECT-PRO. Therefore, we split LOPEX into independent
216 calibration and validation subsets. To minimize risks of an imbalanced distribution of protein content
217 between calibration and validation sets, all dry and fresh samples were pooled together, and subsequently
218 rank ordered based on increasing protein content. Every second sample among this pooled data was
219 selected for calibration and the remaining samples were used for validation. The calibration datasets will
220 be referred to as CALIBRATION while the validation datasets will be identified as VALIDATION, and the
221 combined dataset will be referred to as LOPEX-CALVAL. Dataset mean and range values are provided in
222 Table 1. The Pearson correlation coefficients for log-transformed biochemical contents of fresh leaf
223 samples are presented in Figure 1 (Section 5.a).

224

225 Table 1. Statistical summary, mean values and ranges, of dry matter and protein contents and
 226 concentration for fresh and dry samples included in the CALIBRATION and VALIDATION datasets.

Name	No. of samples	<i>LMA</i> (mg.cm ⁻²)	Proteins (mg.cm ⁻²)	Protein concentration (%DW)
CALIBRATION				
Dry	23	5.84 (2.35-9.07)	0.78 (0.38-1.35)	14.32 (7.31-25.22)
Fresh	33	5.29 (2.58-13.69)	0.66 (0.17-1.23)	13.66 (5.02-26.06)
VALIDATION				
Dry	26	5.89 (2.55-16.58)	0.77 (0.15-1.37)	13.98 (5.02-26.06)
Fresh	33	5.18 (1.88-10.88)	0.69 (0.29-1.22)	14.64 (6.97-28.94)

227

228 b. Data for estimation of *LMA* from PROSPECT-PRO inversion

229 Second dataset was assembled to test the capability of PROSPECT-PRO to estimate *LMA* as the
 230 combination of leaf proteins plus *CBC* contents in comparison to the previous PROSPECT-D version (Féret
 231 et al., 2017). For this, we combined six additional datasets that do not include destructive measurements
 232 of leaf proteins: ANGERS, HYYTIALA, ITATINGA, NOURAGUES, PARACOU and LOPEX-Full (Féret et al., 2019)
 233 (see Table 2 for *EWT* and *LMA* statistics). Note that LOPEX-Full includes all individual measurements of
 234 leaf optical properties, i.e., 330 measurements of *LMA* and *EWT* for fresh leaves (66 fresh samples with
 235 five repetitions), whereas the LOPEX CALIBRATION and VALIDATION datasets contain averages of these
 236 five repetition and their corresponding mean protein contents (for more details see Hosgood et al., 1994).

237
 238

239 Table 2. Statistical summary, mean values and ranges, of water and dry matter contents for
 240 experimental datasets used to validate *LMA* estimations from the PROSPECT-PRO inversion.

Name	No. of samples	<i>EWT</i> (mg.cm ⁻²)	<i>LMA</i> (mg.cm ⁻²)
ANGERS	308	11.47 (4.40 – 34.00)	5.12 (1.66 – 33.1)
HYYTIALA	96	9.16 (3.68 – 23.73)	6.27 (2.76 – 15.77)
ITATINGA	415	14.44 (2.20 – 20.20)	10.24 (6.90 – 14.70)
LOPEX-Full	330	11.13 (0.29 – 52.49)	5.30 (1.71 – 15.73)
NOURAGUES	262	11.73 (3.20 – 38.10)	10.81 (3.10 – 21.10)
PARACOU	272	<i>N/A</i> (<i>N/A</i> – <i>N/A</i>)	12.32 (5.28 – 25.56)

241

242 4. METHODS

243 a. PROSPECT forward modelling and inversion

244 In forward mode, PROSPECT simulates leaf optical properties based on a set of biophysical and
 245 biochemical properties (N_{struct} and leaf biochemistry). In inverse mode, the optimal set of biophysical
 246 and biochemical properties can be identified via a variety of methods, for example, using a merit function
 247 that minimizes the difference between measured and simulated LOP. A common inversion procedure is
 248 based on the numerical minimization of the sum of weighted square errors over all available spectral
 249 bands (Baret and Buis, 2008; Féret et al., 2019). The minimized merit function M , using both reflectance
 250 and transmittance properties, is expressed as follows:

251

$$M(N_{struct}, \{C_i\}_{i=1:p}) = \sum_{\lambda=\lambda_1}^{\lambda_n} [W_{R,\lambda} \times (R_\lambda - \hat{R}_\lambda)^2 + W_{T,\lambda} \times (T_\lambda - \hat{T}_\lambda)^2], \quad (1)$$

252

253 where p is the number of chemical constituents accounted for by PROSPECT and retrieved during the
254 inversion, C_i the biochemical content per unit of leaf surface for a constituent i , λ_1 and λ_n are the first
255 and last wavebands entering the inversion, R_λ and T_λ are the experimental reflectance and transmittance
256 measured at waveband λ , \hat{R}_λ and \hat{T}_λ are the reflectance and transmittance simulated by PROSPECT with
257 $\{N_{struct}, \{C_i\}_{i=1:p}\}$ as input variables, and $W_{R,\lambda}$ and $W_{T,\lambda}$ are the weights applied to the squared
258 difference between experimental and simulated reflectance and transmittance, respectively. Eq. (1) can
259 be used to estimate all input variables, or just their limited subset, if a prior information or arbitrary values
260 of some variables are known. In this study, the values of $W_{R,\lambda}$ and $W_{T,\lambda}$ were set to 0 for non-selected and
261 1 for selected spectral bands, giving all the selected wavelengths the same importance.

262

263 b. Calibration of PROSPECT-PRO

264 The previous PROSPECT versions (Féret et al., 2017, 2008) had the specific absorption coefficients of *LMA*
265 defined by implicitly accounting for various dry matter constituents. Since the distinction of all individual
266 *LMA* constituents is beyond the scope of this study, our primary objective is to replace *LMA* by nitrogen-
267 containing proteins and *CBC* as new leaf input constituents in PROSPECT-PRO. Lignin, cellulose,
268 hemicellulose and non-structural carbohydrates (sugars and starch), were grouped in a single unique input
269 called *CBC*, while the remaining nitrogen-based proteins represent the second standalone input. Please
270 note that from hereafter we refer to the nitrogen-based proteins simply as proteins. Each constituent of
271 *CBC* has a specific carbon content (Ma et al., 2018) but does not contain N. We used both dry and fresh
272 leaf samples in the CALIBRATION dataset to calibrate the specific absorption coefficients corresponding
273 to these two groups of leaf constituents, assuming that *LMA* can be split into protein and other *CBC*
274 contents as follows:

275

$$LMA = Protein\ content + CBC\ content. \quad (2)$$

276

277 where LMA , protein content and CBC content are expressed in mass per leaf surface unit ($\text{mg}\cdot\text{cm}^{-2}$). This
278 ensures conservation of the mass of absorbing materials and allows us to invert PROSPECT-PRO for an
279 estimation of LMA as the sum of leaf protein and CBC contents.

280 Absorption $k(\lambda)$ of a compact leaf layer at wavelength λ , for a given mesophyll structural parameter
281 N_{struct} , is in every PROSPECT model defined as:

282

$$k(\lambda) = \frac{\sum_i K_{spe,i}(\lambda) \times C_i}{N_{struct}}, \quad (3)$$

283

284 where $K_{spe,i}(\lambda)$ is the specific absorption coefficient of a constituent i , and C_i is its corresponding content.

285 In PROSPECT-D, only two input constituents contribute to absorption in the spectral region from 1000 to
286 2500 nm (focus of this study): water (EWT), with a negligible absorption before 1100 nm, and dry matter
287 (LMA), with a constant absorption between 1000 and 1200 nm. Additional leaf constituents accounted
288 for in PROSPECT-D and absorbing in the VIS-NIR spectral domain up to 1100 nm are brown pigments (Ustin
289 and Jacquemoud, 2020). The brown pigments, observed in senescent leaves as result from oxidation and
290 polymerization of cell constituents, are excluded from our analysis because they exhibit only a minor
291 absorption between 1000 and 1100 nm. Therefore, Eq. (3) can be for the purpose of PROSPECT calibration
292 between 1000 and 2500 nm written as follows:

293

$$k(\lambda) = \frac{K_{spe,EWT}(\lambda) \times C_{EWT} + K_{spe,LMA}(\lambda) \times C_{LMA}}{N_{struct}}. \quad (4)$$

294

295 Following the equivalence in Eq. (2), the contribution of LMA to the total absorption can then be
296 decomposed into the proteins and CBC as:

297

$$K_{spe,LMA}(\lambda) \times C_{LMA} = K_{spe,PROT}(\lambda) \times C_{PROT} + K_{spe,CBC}(\lambda) \times C_{CBC}, \quad (5)$$

298

299 where $K_{spe,PROT}(\lambda)$ is specific absorption coefficient for proteins, $K_{spe,CBC}(\lambda)$ is specific absorption
300 coefficient for the *CBC* (both in $\text{cm}^2 \cdot \text{mg}^{-1}$), and C_{PROT} and C_{CBC} are the corresponding contents (in $\text{mg} \cdot \text{cm}^{-2}$), respectively. We assume that $K_{spe,LMA}$ in PROSPECT-D is accurately calibrated, and we use it as a
301 constraint for the calibration of $K_{spe,PROT}$ and $K_{spe,CBC}$, based on Eq. (5).
302

303 The calibration of PROSPECT-PRO followed the commonly-used two-step process (Féret et al., 2017, 2008;
304 Jacquemoud and Baret, 1990) that included the additional constraint, i.e. the decomposition of absorption
305 for *LMA* into proteins and *CBC*. First, we determined the leaf structure parameter $N_{struct,j}$ of each leaf j
306 in the calibration datasets. $N_{struct,j}$ was estimated based on a multivariate iterative optimization,
307 simultaneously with three absorption coefficients, using reflectance and transmittance values measured
308 at three wavelengths corresponding to the minimum absorptance (λ_1), maximum reflectance (λ_2), and
309 maximum transmittance (λ_3) of the leaf (Jacquemoud et al., 1996). These values are generally located on
310 the NIR reflectance and transmittance plateau. The iterative optimization was performed using the
311 following merit function:

312

$$M_{leafN} \left(N_{struct,j}, k(\lambda_1), k(\lambda_2), k(\lambda_3) \right) = \sum_{l=1}^3 \left[\left(R_{meas,j}(\lambda_l) - R_{mod} \left(N_{struct,j}, k(\lambda_l) \right) \right)^2 + \left(T_{meas,j}(\lambda_l) - T_{mod} \left(N_{struct,j}, k(\lambda_l) \right) \right)^2 \right], \quad (6)$$

313

314 where $R_{meas,j}(\lambda_l)$ and $T_{meas,j}(\lambda_l)$ are measured directional-hemispherical reflectance and transmittance
315 of leaf j at wavelength λ_l , R_{mod} and T_{mod} are the respective modeled values, and $k(\lambda)$ is the specific

316 absorption coefficient of a compact layer at the wavelength λ , which is being adjusted simultaneously
 317 with $N_{struct,j}$.
 318 In the second step, $K_{spe,PROT}$ and $K_{spe,CBC}$ were computed by inverting PROSPECT-PRO and using the
 319 CALIBRATION dataset for each spectral band of interest independently. In order to include the constraint
 320 defined in Eq. (5), the minimization algorithm was executed in two consecutive phases, which were
 321 embedded (nested) in a unique iterative procedure for optimization of $K_{spe,PROT}(\lambda)$ and $K_{spe,CBC}(\lambda)$.
 322 During the first phase, the estimated value of $K_{spe,CBC}(\lambda)$ was computed by resolving a system of the
 323 following linear equations:

$$324 \quad K_{spe,CBC}(\lambda) \begin{bmatrix} C_{CBC,1} \\ C_{CBC,2} \\ \vdots \\ C_{CBC,n} \end{bmatrix} = \begin{bmatrix} K_{spe,LMA}(\lambda) \times C_{LMA,1} - K_{spe,PROT}(\lambda) \times C_{PROT,1} \\ K_{spe,LMA}(\lambda) \times C_{LMA,2} - K_{spe,PROT}(\lambda) \times C_{PROT,2} \\ \vdots \\ K_{spe,LMA}(\lambda) \times C_{LMA,n} - K_{spe,PROT}(\lambda) \times C_{PROT,n} \end{bmatrix}, \quad (7)$$

325
 326 where $K_{spe,PROT}(\lambda)$ is initially set to a user-defined value, then updated at each iteration. In the second
 327 phase, the optimal value of $K_{spe,PROT}(\lambda)$ was adjusted by following the strategy defined by the sequential
 328 quadratic programming algorithm (Fletcher, 2000). We minimized the following merit function J per
 329 wavelength (λ):

$$330 \quad J(\{K_{spe,i}(\lambda)\}_{i=1:n}) \\
 = \sum_{j=1}^n \left[\left(R_{meas,j}(\lambda) - R_{mod,j}(N_{struct,j}, k(\lambda)) \right)^2 \right. \\
 \left. + \left(T_{meas,j}(\lambda) - T_{mod,j}(N_{struct,j}, k(\lambda)) \right)^2 \right], \quad (8)$$

331

332 with $k(\lambda)$ defined as follows:

333

$$k(\lambda) = \frac{K_{spe,EWT}(\lambda) \times C_{EWT} + K_{spe,PROT}(\lambda) \times C_{PROT} + K_{spe,CBC}(\lambda) \times C_{CBC}}{N_{struct}}, \quad (9)$$

334

335 where $K_{spe,PROT}(\lambda)$ is the only unknown term and $K_{spe,CBC}(\lambda)$ is taken from the previous phase. In other
336 words, the $K_{spe,CBC}(\lambda)$ and $K_{spe,PROT}(\lambda)$ values were updated during each iteration until the procedure
337 found the optimum for $K_{spe,PROT}(\lambda)$, and then the final value of $K_{spe,CBC}(\lambda)$ was obtained from Eq. (7),
338 using the optimized $K_{spe,PROT}(\lambda)$.

339 This calibration procedure, expecting correctly defined $K_{spe,LMA}$, was performed within the spectral
340 domain of 1000 to 2500 nm, using the same leaf refractive index and the specific absorption coefficients
341 for *EWT* as defined in PROSPECT-D. The calibration of specific absorption coefficients in the NIR domain is
342 challenging due to a generally low absorption and a possibly significant uncertainty in measured leaf
343 optical properties within this spectral domain. When calibrating the specific absorption for *LMA*, Féret et
344 al. (2008) set the specific absorption coefficients of *LMA* to a constant value for wavelengths < 1200 nm.
345 Here, we fitted an exponential function to the start of absorption of proteins, ensuring smooth transition
346 between the two non-absorptive and absorptive spectral domains, corresponding to the spectral domain
347 between 1440 and 1490 nm. Subsequently, the specific absorption coefficients for *CBC* between 1000 and
348 1200 nm were adjusted according to the specific absorption coefficients of *LMA* from PROSPECT-D, by
349 applying a multiplicative factor corresponding to the average ratio between *LMA* and *CBC* in the
350 CALIBRATION dataset.

351

352 c. Global sensitivity analysis of PROSPECT-PRO

353 A global sensitivity analysis (GSA) was carried out for PROSPECT-PRO to quantify the contribution of
354 proteins and *CBC* constituents to the overall spectral signal. Using a GSA the driving variables of a radiative
355 transfer model can be identified by fully exploring the input parameter space (Verrelst et al., 2019b; Wang
356 et al., 2015). The Matlab software tool GSAT (Cannavó, 2012), which includes Fourier amplitude sensitivity
357 testing (FAST) analysis and Sobol's method for calculation of the first-order sensitivity coefficients was
358 applied on PROSPECT-PRO simulations from 1000 nm to 2500 nm carried out with the following realistic
359 input parameter ranges for fresh leaves: $N_{struct} \sim 1-2$ (unitless), $EWT \sim 0.001-0.015$ cm, protein content
360 (C_p) $\sim 0-0.003$ g/cm² and *CBC* content $\sim 0-0.01$ g/cm². The remaining PROSPECT-PRO input parameters,
361 i.e. chlorophyll content, total carotenoid content, anthocyanin content and brown pigment content, were
362 fixed to arbitrary values since they manifest no absorption between 1000-2500 nm.

363

364 d. Optimal spectral domains for estimation of protein and *CBC* content

365 In previous studies (Colombo et al., 2008; Féret et al., 2008; Jacquemoud et al., 1996), a PROSPECT model
366 inversion was performed with an iterative optimization of the merit function defined in Eq. (8) over the
367 entire optical domain or broad spectral intervals (e.g., VIS-NIR when retrieving leaf pigments and NIR-
368 SWIR when retrieving *EWT* and *LMA*), using a uniform weight of 1 across all spectral bands. Féret et al.
369 (2019) showed the importance of identifying optimal spectral domain for the accurate estimation of *LMA*
370 and, to a lesser extent, *EWT*. Investigating a number of spectral ranges between 1000 and 2400 nm, they
371 recommended determination of *EWT* and *LMA* with an iterative optimization of leaf optical properties
372 between 1700 and 2400 nm. Although proteins are part of *LMA*, the hypothesis that proteins and *LMA*
373 share the same optimal retrieval spectral domain needs appropriate testing. Moreover, the fact that
374 protein absorption is expressed in a number of narrow SWIR spectral features (Curran, 1989; Fourty et al.,
375 1996) suggests that proteins and *CBC* may have slightly different optimal retrieval spectral domains
376 compared to *LMA*.

377 The procedure suggested by Féret et al. (2019) is limited to the identification of an optimal contiguous
378 spectral domain. As such, it is unable to identify spectral features located in narrow non-contiguous
379 domains separated by suboptimal spectral intervals of varying lengths. To be able to identify also the non-
380 contiguous optimal spectral domains, we adapted a sequential forward feature selection (SFS) technique
381 (Kudo and Sklansky, 2000; Marcano-Cedeno et al., 2010). SFS is a bottom-up search procedure that starts
382 from an empty feature set and gradually adds features selected based on a minimization criterion. In our
383 study, each spectral feature was defined as a set of 20 spectral bands of the original leaf optical properties
384 with the 1 nm spectral sampling, which allowed for a large number of explored spectral bands and made
385 the computation of the iterative optimization feasible. This way, we created 50 spectral features between
386 1400 and 2399 nm and applied SFS on these spectral features. We first identified the spectral feature
387 leading to minimum root mean square error (*RMSE*) when estimating either proteins or *CBC* from the
388 experimental data. Then we searched for the spectral feature leading to minimum *RMSE*, if combined
389 with the previously identified spectral feature, until all spectral features were tested. At the final step, all
390 features were sequentially added and ranked based on the search for minimum *RMSE*, and the full domain
391 1400 and 2399 nm was used for inversion with the original spectral data.

392 As the CALIBRATION dataset was dedicated to the calibration of the specific absorption coefficients of
393 proteins and *CBC*, the accuracy and robustness of PROSPECT inversion for retrieval of these leaf
394 constituents had to be assessed with the independent VALIDATION dataset. Use of the CALIBRATION
395 dataset would be logically defrauded and scientifically incorrect. The selection of optimal spectral domains
396 is not considered as a part of the calibration procedure but expected to be performed before or during a
397 PROSPECT inversion. As such, its robustness would be best ensured when performed on an independent
398 dataset. Unfortunately, due to a limited size of available experimental data, the sample pool could not be
399 reasonably split into three independent CALIBRATION, FEATURE SELECTION and VALIDATION parts.
400 Therefore, the optimal spectral domains were identified by applying SFS on the VALIDATION dataset.

401 Once the specific optimal spectral domains for estimation of proteins and *CBC* were identified, we
402 compared their estimates with results obtained for the spectral domain between 1700 and 2400 nm,
403 identified as optimal for the estimation of *LMA* and *EWT* by Féret et al. (2019). Finally, we compared the
404 performances of PROSPECT-PRO and PROSPECT-D for the estimation of *LMA* using the 1700-2400 nm
405 spectral domain, and by inverting PROSPECT-PRO over the SFS identified optimal spectral domains for
406 proteins and *CBC* estimations and calculating *LMA* from Eq. (2). This model comparison was carried out
407 for the six additional datasets listed in Table 2.

408 The normalized *RMSE* (*NRMSE* expressed in %) was computed to appraise the difference between the
409 measured and estimated leaf constituents retrieved from the different datasets:

410

$$NRMSE = \frac{1}{\overline{X_{meas}}} \sqrt{\frac{\sum_{j=1}^n (X_{meas,j} - X_{mod,j})^2}{n}}, \quad (10)$$

411

412 where $X_{meas,j}$ is the measured value and $X_{mod,j}$ is the values estimated by model inversion for a leaf j ,
413 $\overline{X_{meas}}$ is the mean value of the constituent, and n is the number of samples.

414 All inversions and optimal feature selections were performed with the prospect R package (Féret and
415 Boissieu, 2020), which uses the nonlinear constrained multivariable minimization function of the pracma
416 R package (Borchers, 2019).

417 e. Performances of PROSPECT-D and PROSPECT-PRO in forward modelling

418 We compared the performances of PROSPECT-D and PROSPECT-PRO for the forward simulation of leaf
419 optical properties, using the structure parameter N_{struct} obtained from inversion and the corresponding
420 biochemical constituents measured in laboratory. This statistical analysis was undertaken to reveal
421 spectral domains impacted by high levels of uncertainty, which is relevant for possible future hybrid
422 inversion applications involving machine learning algorithms trained with PROSPECT-PRO simulated data

423 (e.g., Verrelst et al., 2015 and 2019a). The comparison was performed by computing the per-wavelength
 424 spectral $RMSE$ between measured and simulated reflectance and transmittance of fresh and dry samples
 425 from the VALIDATION dataset, and also systematic ($RMSE_S$) and unsystematic ($RMSE_U$) parts of $RMSE$
 426 (Willmott et al., 1985) defined as:

427

$$RMSE_S = \sqrt{\frac{\sum_{j=1}^n (\hat{X}_{meas,j} - X_{mod,j})^2}{n}}, \quad (11)$$

428

429 and

430

$$RMSE_U = \sqrt{\frac{\sum_{j=1}^n (\hat{X}_{meas,j} - X_{meas,j})^2}{n}}, \quad (12)$$

431

432 where $\hat{X}_{meas,j}$ is an ordinary least square estimate of $X_{meas,j}$, and n is the number of samples. Eqs. (11)

433 and (12) are a complete partitioning of $RMSE$ as follows:

434

$$RMSE^2 = RMSE_U^2 + RMSE_S^2 \quad (13)$$

435

436 The $RMSE_S$ corresponds to the linear bias of the estimate produced by the model itself, while the $RMSE_U$

437 corresponds to a measure of precision of the model and it is driven by uncertainties in input data.

438

439 f. Estimation of the carbon-nitrogen ratio

440 The carbon:nitrogen (C:N) ratio of plant canopies, crops and crop residues is of great importance for

441 modelling C and N dynamics in natural ecosystem and agricultural systems, as it contains an indicative

442 information about plant growth rate and affects ecosystem response to CO₂ (Reich et al., 2006; Zheng,
443 2009). This C:N ratio is also an indicator of the relative allocation of resources in vegetation, an indicator
444 of potential decomposition rate of litter and an important factor promoting soil organic carbon
445 accumulation (Zhou et al., 2019). Thus, we tested the possibility of using the *CBC:Proteins* ratio, estimated
446 from PROSPECT-PRO inversion, as a proxy for the C:N ratio of leaf samples in the LOPEX dataset. We
447 established a linear model to estimate the C:N ratio based on the *CBC:Proteins* ratio as measured in the
448 fresh samples of the CALIBRATION dataset. We then applied this linear relationship on *CBC:Proteins* ratio
449 retrieved from leaf optical properties through PROSPECT-PRO inversion to estimate the C:N ratio for all
450 samples in both CALIBRATION and VALIDATION datasets.

451

452 5. RESULTS

453 a. Correlations among biochemical constituents of fresh leaves in LOPEX-CALVAL data

454 Since descriptive statistics computed for leaf constituents of fresh samples in the LOPEX-CALVAL dataset
455 revealed that a majority of them does not follow the Gaussian distribution, they were log-transformed by
456 applying the natural logarithm. The subsequent correlation analysis performed on log-transformed data
457 indicated potential relationships between individual biochemical compounds. Figure 1 shows the Pearson
458 correlation coefficients (r) for tested constituents, including the C:N ratio. Proteins are not included, as
459 they were derived directly from N measurements. The coefficients highlight strong and statistically
460 significant relationships between carbon (C), hydrogen (H), oxygen (O), lignin, cellulose and *LMA*. Nitrogen
461 (N) content is moderately correlated to chlorophyll $a+b$ content (CHL), C, H, O, *LMA* and *EWT*. The
462 moderate correlation between CHL and N ($r = 0.51$) indicates a modest capacity of CHL to estimate N
463 across species in the LOPEX dataset. Finally, the C:N ratio was found to be moderately positively correlated
464 with *LMA*, C, H, O and individual *CBC* except starch, and poorly negatively correlated with the N content
465 ($r = -0.36$).

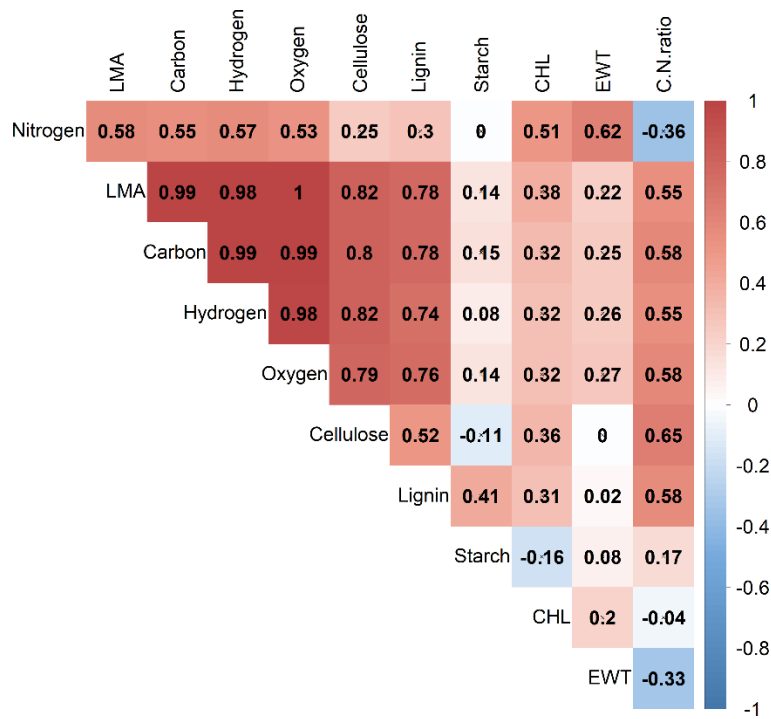


Figure 1. Pearson correlation coefficients computed among log-transformed contents of biochemical constituents of fresh leaf samples in the LOPEX-CALVAL dataset.

b. Calibration of PROSPECT-PRO

A Matlab version of the new PROSPECT-PRO model is downloadable from the following GitLab repository:

https://gitlab.com/jbferet/prospect_pro_matlab. The R package including PROSPECT-D is installable

from the GitLab repository: <https://jbferet.gitlab.io/prospect/>. The specific absorption coefficients

derived for leaf proteins and *CBC* are displayed in Figure 2. Most of the absorption features reported by

Curran (1989) and Fourty et al. (1996) correspond with the local maxima of the obtained specific

absorption of proteins, although some of them are spectrally shifted towards shorter or longer

wavelengths.

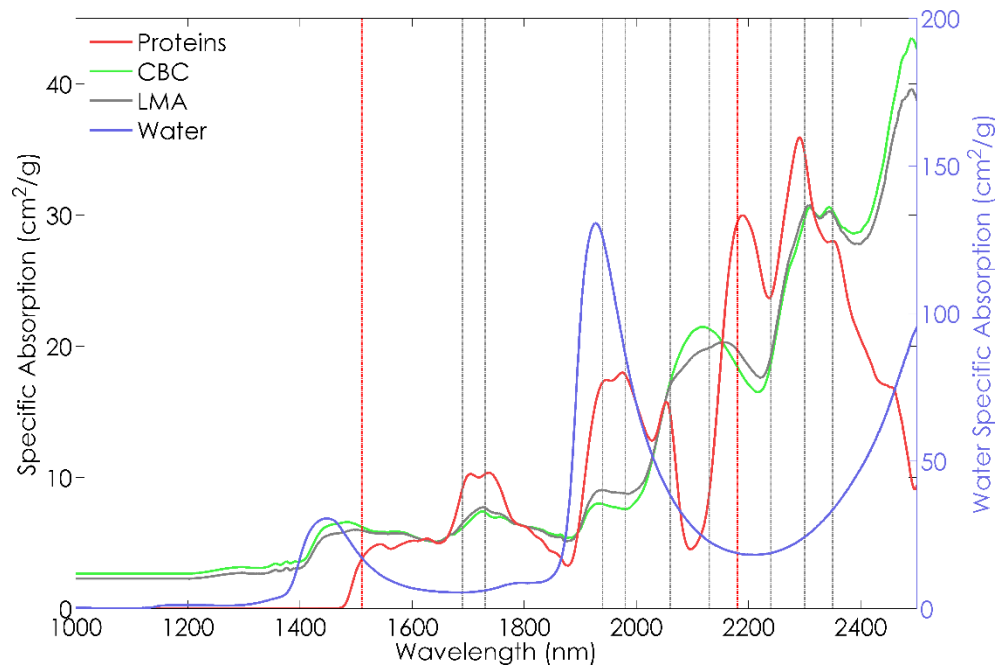


Figure 2. Specific absorption coefficients for proteins and *CBC* obtained from calibration of PROSPECT-PRO using the CALIBRATION dataset. The coefficient corresponding to *LMA* and water, used in PROSPECT-D, are displayed for comparison. Vertical dashed lines indicate wavelengths of absorption features linked to proteins by Curran (1989) and Fourty et al. (1996) (red = major and grey = minor absorption features).

477

478 c. Sensitivity of leaf optical properties to proteins and *CBC*

479 Results of GSA for PROSPECT-PRO simulated leaf reflectance and transmittance were nearly identical.

480 Therefore, we present in Figure 3 only the outcomes for reflectance and absorptance of fresh and dry

481 leaves. GSA identified the spectral regions that contain absorption peaks of proteins (> 1400 nm), but it

482 also shows their relatively low contribution to the spectral signal in these wavelengths, in particular for

483 fresh leaves. *CBC* play a larger role in driving leaf reflectance and absorptance, with their highest relevance

484 in SWIR, especially above 2000 nm. Yet, the key driving input parameters of PROSPECT-PRO forward

485 simulations of fresh leaf reflectance are the N_{struct} parameter and *EWT*. As expected, N_{struct} has no

486 impact on leaf absorptance. Water and *CBC* are the dominant absorbers of fresh and dry leaves,

487 respectively, in the SWIR domain. Although absorption features of proteins between 1600 and 1800 nm
 488 and between 2100 and 2300 nm are subtle, GSA confirms that these spectral domains have the greatest
 489 potential for retrieval activities for both dry and fresh leaves.
 490 Nevertheless, data of high spectral sampling and resolution with a sufficiently high signal-to-noise (SNR)
 491 and an efficient identification of the most optimal retrieval wavelengths within these spectral domains
 492 are required to enable the separation of all influencing constituents, especially in future efforts when
 493 upscaling the retrieval methods from the leaf to the top-of-canopy level.
 494

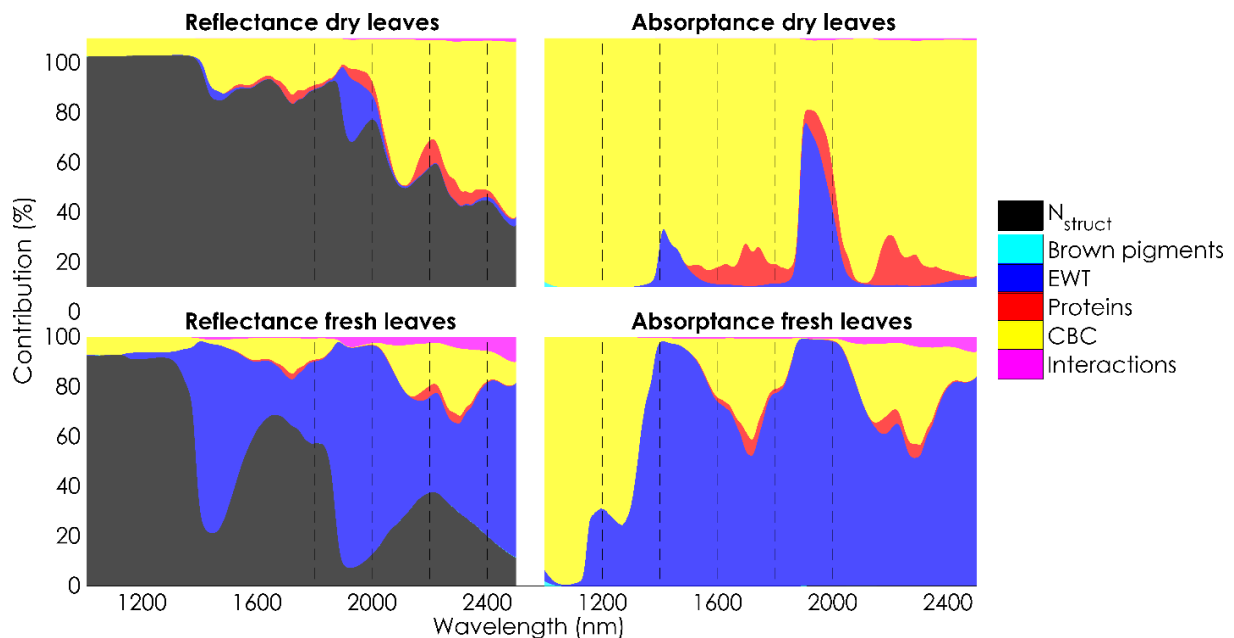


Figure 3. Global sensitivity analysis of PROSPECT-PRO input parameters, i.e. leaf structure (N_{struct}), leaf water content (EWT), protein content, carbon-based constituents (CBC) and brown pigments, simulating reflectance (left) and absorptance (right) of dry (top) and fresh leaves (bottom), including reciprocal interactions in a typical bifacial leaf. The y-axis ('contribution') quantifies the first-order effects, implying the contribution of each tested input to the modelled output variance.

495

496

d. Optimal wavelengths for PROSPECT-PRO retrieval of proteins and CBC content

497 Figure 4 shows the *NRMSE* for the estimation of protein and *CBC* contents by inverting PROSPECT-PRO
498 over the VALIDATION dataset and applying the SFS optimization procedure on spectral features with 20
499 nm width within the spectral domain between 1400 and 2400 nm. The optimal estimation of proteins was
500 obtained with three spectral features encompassing the spectral domains between 2100 and 2139 nm,
501 and between 2160 and 2179 nm. The later one is located next to the strong protein absorption feature
502 centered at 2180 nm, as noted by Curran (1989), Fourty et al. (1996) and Wang et al. (2015). The optimal
503 estimation of *CBC* was obtained when selecting thirteen 20 nm wide spectral features, four of them
504 located between 1480 and 1800 nm, and nine of them between 2040 and 2399 nm. Inclusion of additional
505 spectral features did not lower accuracy for the *CBC* estimations, except for spectral domains between
506 1400 and 1439 nm, and between 1860 and 2000 nm that correspond to the two main water absorption
507 features. In the case of proteins, inclusion of additional spectral information besides the identified optimal
508 spectral features led to an increased *NRMSE*. The maximum *NRMSE* increase was obtained when including
509 spectral information corresponding to the main absorption peak of water between 1880 and 2000 nm.
510

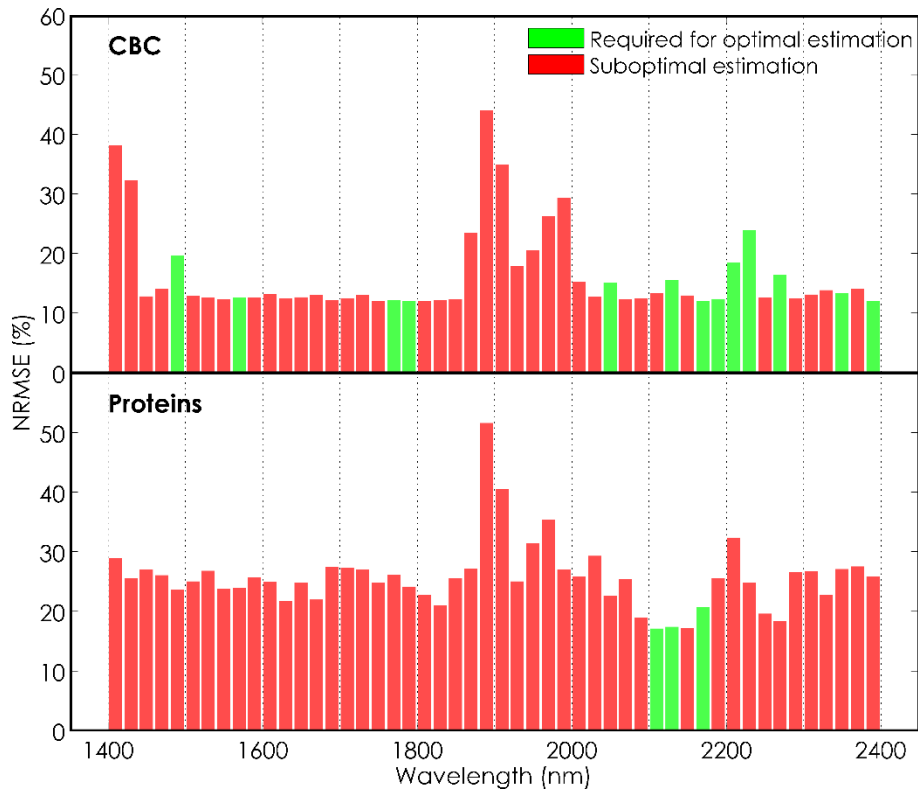


Figure 4. *NRMSE* (%) obtained for the estimation of protein and *CBC* contents with a PROSPECT-PRO inversion applied on the VALIDATION dataset using the SFS method (green = spectral features required to reach the minimal *NRMSE* and red = suboptimal spectral domains increasing *NRMSE*).

511

512 Figure 5 illustrates the evolution of *NRMSE* as the number of spectral features selected with SFS for the
 513 full VALIDATION dataset, as well as for the dry samples and fresh samples separately, increases. The
 514 *NRMSE* development fluctuates but stays relatively similar until 40 to 45 spectral features when
 515 estimating protein contents for both types of leaves. It dramatically increases for fresh leaves once
 516 spectral features located on the main absorption peak of water are included. Similar results were obtained
 517 for *CBC*. The errors remain relatively similar around the optimal performance until 40 spectral features,
 518 and also strongly increase when including spectral domains of water absorption.

519

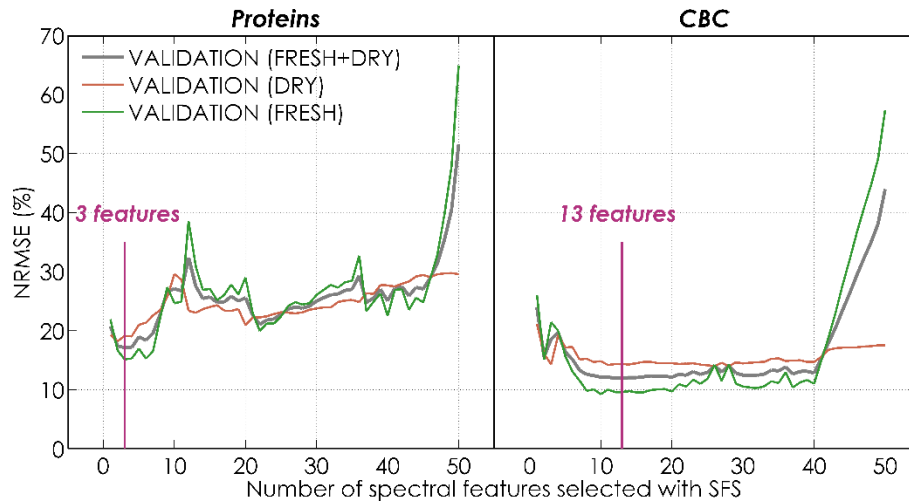


Figure 5. Evolution of *NRMSE* with an increasing number of spectral features selected with SFS when estimating proteins (left) and *CBC* (right) (grey line = *NRMSE* computed for all samples in the VALIDATION dataset, red line = *NRMSE* computed for dry samples and green line = *NRMSE* computed for fresh samples in the VALIDATION dataset. The number of features leading to minimum *NRMSE* for all VALIDATION samples is indicated with the violet vertical line.

520

521 e. PROSPECT-PRO validation by retrieval of leaf protein and *CBC* contents

522 Comparison between laboratory measured and PROSPECT-PRO estimated protein, *CBC* and *LMA* contents
 523 for the VALIDATION dataset is shown in Figure 6. The simultaneous retrievals of leaf protein and *CBC*
 524 contents from inversions were performed either over the spectral region from 1700 to 2400 nm or over
 525 the optimal spectral features identified with the SFS method. The R codes and data used to produce these
 526 results are available in the prospect R package (Féret and Boissieu, 2020).

527 The results illustrate the importance of selected optimal spectral features for accuracy of leaf constituent
 528 estimates, especially when analyzing fresh leaf samples. The estimation of proteins has a slightly higher
 529 uncertainty than the estimation of *CBC* and *LMA*, which can be explained by a lower contribution of
 530 proteins to the spectral signal (Figure 3). Additionally, a lower accuracy obtained for the estimation of
 531 protein content from dry leaves is caused mainly by a single sample of dry maple (*Acer pseudoplatanus L*)

532 leaf. The estimation of *LMA* based on the inversion of PROSPECT-D using the spectral domain between
 533 1700 and 2400 nm produced results similar to those obtained with PROSPECT-PRO (*NRMSE* = 14.2% for
 534 dry leaves and *NRMSE* = 34.3% for fresh leaves).
 535

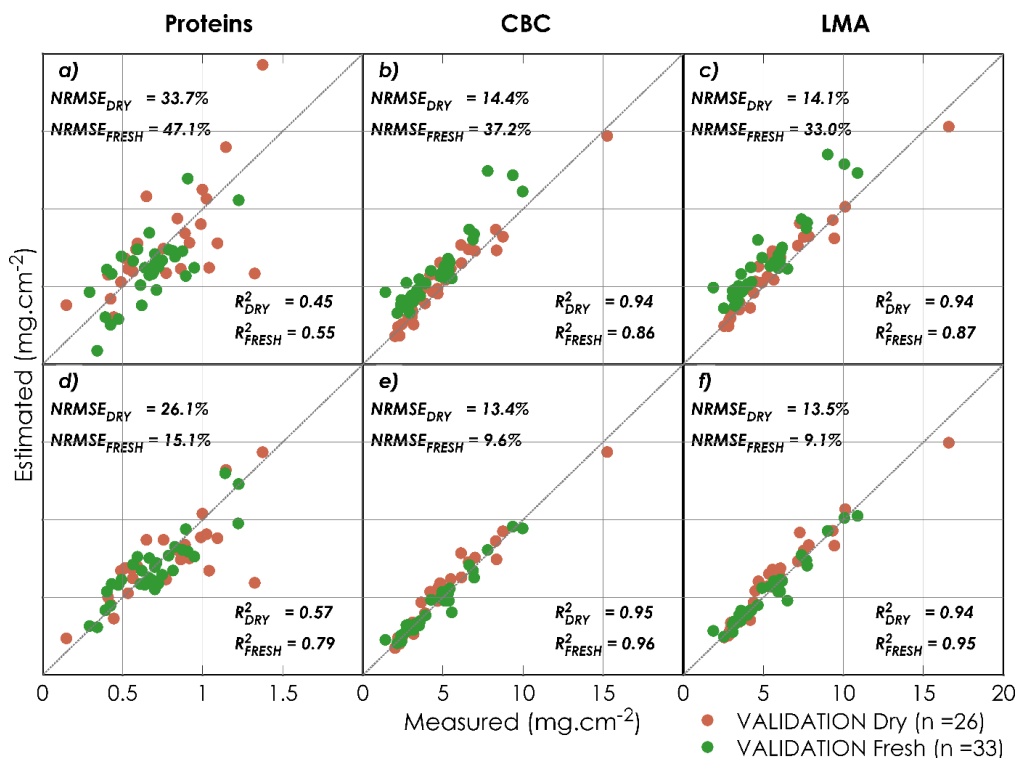


Figure 6. Comparison between laboratory measured and PROSPECT-PRO estimated leaf protein, *CBC* and *LMA* (proteins + *CBC*) contents obtained for the VALIDATION dataset using either the spectral range from 1700 to 2400 nm (a to c) or the optimal spectral features identified with the SFS method (d to f) (see Figure 4 in Section 5.d).

536
 537 f. PROSPECT-PRO and PROSPECT-D compatibility assessed via estimation of *LMA* and
 538 *EWT*
 539 Overall, the decomposition of *LMA* into protein and *CBC* contents estimated by the PROSPECT-PRO over
 540 the SFS optimized spectral regions slightly outperformed the *LMA* estimations obtained with the

541 PROSPECT-D inversion over the optimal spectral domain 1700-2400 nm identified by Féret et al. (2019)
542 (Figure 7). When analyzing the results per dataset, inversion of PROSPECT-PRO using the optimal spectral
543 domain for protein and *CBC* content retrievals resulted in a decreased *NRMSE* for *LMA* estimations for
544 five out of eight datasets (including the VALIDATION Dry and VALIDATION Fresh datasets). Very similar
545 performances were found for ITATINGA. The increase in *NRMSE* observed for ANGERS was caused by two
546 samples of Holly osmanthus (*Osmanthus heterophyllus*), characterized by high *LMA* and *EWT* values, while
547 the remaining samples showed comparable estimates. However, this influence of high *EWT* or *LMA*
548 contents was not a general feature, as this effect was not observed in case of other datasets that include
549 samples with high *LMA*. The less accurate performances observed for HYTIALA corresponds to an
550 increased uncertainty distributed among all samples. Finally, when combining all datasets described in
551 Table 2, the indirect estimation of *LMA* from the inversion of PROSPECT-PRO using the optimal spectral
552 features was slightly improved, with a 1.8% decrease in *NRMSE* and comparable R^2 across all data sets.
553 Still, the differences observed among independent datasets suggest that the optimal spectral features
554 computed for the VALIDATION dataset do not correspond exactly with the optimal spectral features for
555 other datasets. Finally, the version of the model did not influence the estimation of *EWT* significantly.
556 Inversions of PROSPECT-D and PROSPECT-PRO conducted over the same spectral domain (1700-2400 nm)
557 resulted in similar outcomes ($NRMSE = 11.9$ and $R^2 = 0.91$ for both model inversions when combining all
558 datasets). The results confirm the compatibility between PROSPECT-D and PROSPECT-PRO.
559

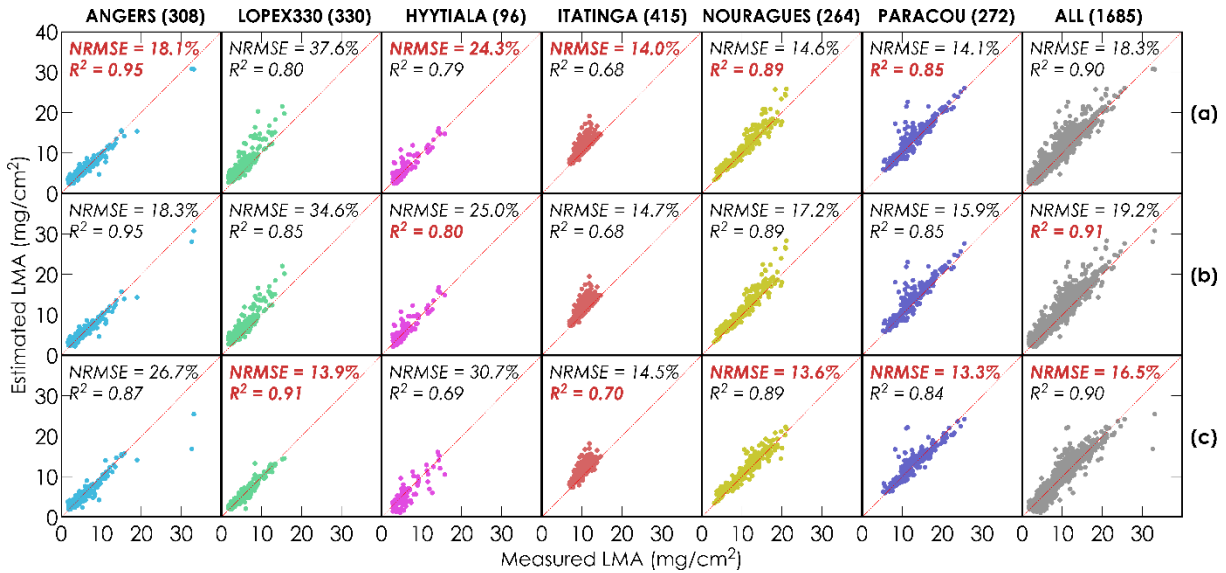


Figure 7. Comparison between measured *LMA* and its corresponding estimations by inversion of a) PROSPECT-D (1700-2400 nm), b) PROSPECT-PRO (1700-2400 nm), and c) PROSPECT-PRO (SFS optimized spectral features for proteins and *CBC*). Values in brackets show the number of samples and red fonts indicate the best achieved results per dataset.

560

561 g. Forward simulations of leaf optical properties

562 Figure 8 displays per-wavelength $RMSE$, $RMSE_S$ and $RMSE_{IJ}$ calculated between measured leaf
 563 reflectance and transmittance and their counterparts produced by PROSPECT-PRO for VALIDATION dry
 564 and fresh samples and also samples of the six independent datasets in Table 2 grouped together. The
 565 input biochemical constituents correspond to the values obtained from laboratory measurements, while
 566 the N_{struct} parameter was obtained from the inversion of PROSPECT-PRO using the spectral information
 567 between 1700 and 2400 nm. Since the independent datasets (Figure 8c and f) do not contain protein and
 568 *CBC* content measurements, the resulting statistical indicators are based on values of protein and *CBC*
 569 contents obtained from the model inversion using the optimal spectral features identified with SFS.
 570 Additionally, the PARACOU dataset was excluded from this analysis, as no measurements of *EWT* were
 571 available.

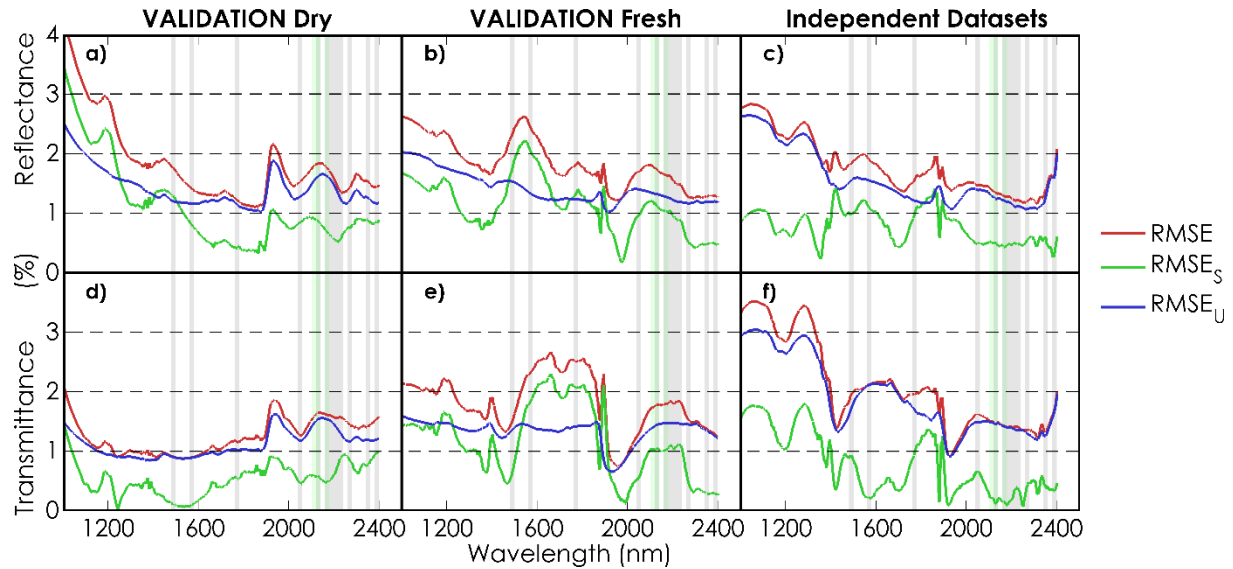


Figure 8. $RMSE$, $RMSE_S$ and $RMSE_U$ between measured and PROSPECT-PRO forward simulated leaf optical properties. The biochemical constituents were measured in laboratory and the N_{struct} parameter was derived by PROSPECT-PRO inversion using the spectral domain from 1700 to 2400 nm. The green and grey areas highlight the respective optimal spectral domains identified by SFS method for estimation of protein and CBC contents.

572

573 VALIDATION dry samples exhibited an $RMSE$ between 1 and 2% in the SWIR, increasing in the NIR to as
 574 high as 4% for reflectance and 2% for transmittance at 1000 nm. The increasing $RMSE$ at shorter
 575 wavelengths and also reflectance $RMSE_S$ higher than $RMSE_U$ may be due to the presence of constituents
 576 similar to brown pigments appearing after the drying process, which were not accounted for during the
 577 simulation, or by residual model inaccuracies at these wavelengths. $RMSE_U$ close to $RMSE$ in the SWIR
 578 region confirms acceptable model accuracy and moderate bias, and shows that the specific absorption
 579 coefficient of LMA as well as proteins and CBC are, in general, able to reassemble dry LOPEX data
 580 measurements very well.

581 In case of fresh VALIDATION samples, the $RMSE$ is generally slightly higher and fluctuates between 1 and
 582 3% of reflectance and transmittance intensities. Nevertheless, $RMSE$ between 2000 and 2400 nm, where

583 most of the optimal spectral features for the estimation of protein and *CBC* contents are located, is
584 smaller, between 1 and 2%. Compared to dry samples, the reflectance *RMSE* between 1000 and 1200 nm
585 is lower, which supports our interpretation of increased NIR *RMSE* in dry samples due to the unaccounted
586 presence of absorbing constituents similar to brown pigment such as products from decay pigments
587 (Proctor et al., 2017). The higher *RMSE* combined with corresponding high *RMSE_S* between c. 1500 and
588 1800 nm suggest that the contribution of water absorption introduces a certain bias in the simulated fresh
589 leaf optical properties.

590 The *RMSE* lower than 2.1% was found for both reflectance and transmittance of the independent
591 datasets for wavelengths > 1500 nm, which is slightly lower than the results obtained for fresh
592 VALIDATION samples. Relatively different and decoupled dynamics between *RMSE* and *RMSE_S* suggest
593 that the contribution of water absorption does not introduce the same bias as observed for fresh
594 VALIDATION samples. The high *RMSE* and *RMSE_J* for both reflectance and transmittance in NIR were
595 not observed for fresh VALIDATION samples, and they do not reassemble by shape the increases observed
596 for dry VALIDATION samples. This may be caused by discrepancies in the protocol for the measurement
597 of the leaf optical properties among datasets. The same analysis performed on the complementary
598 simulations from PROSPECT-D showed very similar results (results not shown).

599

600 h. Estimation of C:N from *CBC*:Proteins ratio retrieved from PROSPECT-PRO inversion

601 The correlation analysis displayed in Figure 1 shows that constituents of *CBC*, such as cellulose and lignin,
602 are strongly correlated with leaf C content. We applied the linear model fitted between *CBC*:Proteins and
603 C:N ratio of the fresh samples in the CALIBRATION dataset (Eq. (14)) to the *CBC*:Proteins ratio PROSPECT-
604 PRO estimates for the VALIDATION datasets:

605

$$C:N = 2.167 \times CBC:Proteins + 1.565. \quad (14)$$

606

607 The results show that the C:N ratio was derived from the *CBC* and proteins PROSPECT-PRO estimates with
 608 a *NRMSE* of 28.1% for dry samples, and an exceptionally low *NRMSE* of 15.7% (R^2 of 0.87) for fresh samples
 609 (Figure 9). The poorer performances for dry samples was strongly driven by a single sample of dry chestnut
 610 (*Castanea sativa*) leaf, and highlights the necessity of further independent verification of the C:N
 611 predictive regression models.

612

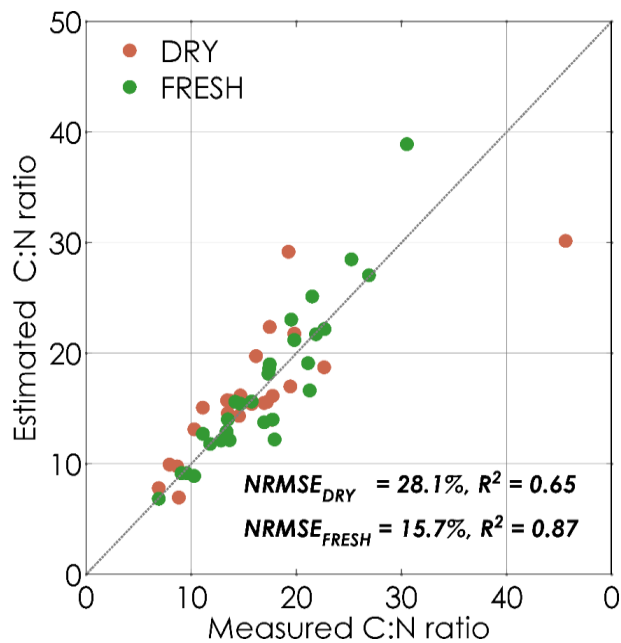


Figure 9. Comparison between the C:N ratio measured in laboratory and the same ratio derived from regression (Eq. (14)) established with PROSPECT-PRO estimated protein and *CBC* contents of dry and fresh samples in the VALIDATION dataset.

613

614 6. DISCUSSION

615 a. Limitations of experimental data available for PROSPECT-PRO calibration and validation

616 Calibration and validation uncertainties are related not only to the physical-empirical model design and
617 mathematical inversion but also to model inputs, i.e. leaf biochemical and optical measurements
618 (Malenovský et al., 2019). Although we used in this study only a single nitrogen-to-protein content
619 conversion multiplicative factor of 4.43, this factor is not constant across all plant species. As reported by
620 Yeoh and Wee (1994), it can range from 3.28 to 5.16, with an average and standard deviation of 4.43 ± 0.40 .
621 This means that the protein content used for calibration and validation of PROSPECT-PRO contains an
622 associated uncertainty that is proportional to the unaccounted variability of this conversion factor. This
623 may also explain the moderately higher uncertainty observed in protein estimates when compared to
624 *LMA* and *CBC* retrievals. Despite this, our results show that the specific absorption coefficients for in vivo
625 proteins are consistent with absorption features derived from dried and ground leaves reported in
626 literature (Curran, 1989). In addition, the protein content estimated through model inversion remained
627 consistent and accurate.

628 Our study only includes one dataset with measured protein and *CBC* content. Therefore, the validation is
629 performed on a limited number of samples ($n=26$ dry and 33 fresh). As such, the errors and uncertainties
630 reported might be strongly affected by just few discrepancies in this low number of samples. As reported
631 in Section 3.a, the presence or absence of a single sample in the calibration dataset significantly impacted
632 the calibration process and the subsequent capability of the model to properly simulate leaf optical
633 properties and to estimate leaf constituents. In the same way, the presence of just few validation samples
634 showing a strong error may lead to difficulties for the statistical interpretation of results obtained from
635 an inversion. In our case, we encountered a lower accuracy for proteins estimation on dry samples. It was
636 caused by a single sample, for which either spectral or biochemical measurement error may have
637 occurred. Additional datasets from various ecosystem types and growing conditions are, therefore,
638 required to test further limitations of PROSPECT inversions, especially for high contents of *EWT* and *LMA*,
639 as identified for a limited set of samples in this study. Finally, more public datasets containing reliable

640 VNIR and SWIR leaf optical properties and corresponding comprehensive and robust laboratory
641 measurements of leaf biochemical constituents are strongly needed. They would also allow us to explore
642 a potential differentiation and inclusion of new ecophysiological important constituents.

643

644 b. Interpretation of GSA

645 Since N_{struct} has no effect on the leaf absorptance (Figure 3), the GSA of the model biochemical input
646 parameters to leaf absorbance can be used to identify the most dynamic absorption regions of leaf
647 constituents. However, it is important to mention that a strong influence of a given constituent does not
648 mean removal of contributions from other constituents with a lower impact. Although *EWT* is the main
649 driver of SWIR absorptance by fresh leaves, the impact of *CBC* is also significant and in case of dry leaves
650 even dominant. Therefore, with the prerequisite of a clean spectral acquisition with a high spectral
651 sampling and resolution, an appropriately parameterized model inversion procedure using selected
652 optimal spectral features can be successful. Hereby, for the model inversion we took advantage of the
653 spectral dynamics of absorbing constituents depicted in Figure 2 and Figure 3. There is a very pronounced
654 increase of protein absorption within the 2100-2200 nm domain, while water absorption is decreasing,
655 and *CBC* absorption reaches first a maximum peak and then starts to decrease. This unique contrasting
656 spectral dynamic, i.e. a change from the local minimum to the local maximum of proteins in contrast to
657 the other two main absorbers showing moderate changes in absorption, explains the high accuracy we
658 achieved when estimating protein content from the identified optimal spectral domain. On the other
659 hand, absorption of *EWT* and proteins both decrease in the spectral region around 2000 nm, and *CBC* and
660 proteins both decrease beyond 2200 nm. These correlated behaviors negatively impact their retrieval
661 accuracy through a model inversion.

662

663 c. Identification of the optimal spectral features

664 The optimal spectral features for estimation of *CBC* and proteins were defined based on the VALIDATION
665 dataset only. The analysis showed that the optimal spectral features selected across all tested datasets
666 were not the same, resulting in an increased *NRMSE* for *LMA* estimates of some experimental datasets
667 (Figure 7). Féret et al. (2019) reached a similar conclusion when identifying specific optimal subdomains
668 for estimation of *EWT* and *LMA*. While Féret et al. (2019) could eventually identify the optimal spectral
669 domain by combining all available datasets, the lack of protein and *CBC* content measurements did not
670 allow us to find the most optimal spectral features across the independent datasets in Table 2.
671 Finally, better performances obtained for the estimation of both proteins and *CBC* from fresh leaf
672 measurements are somewhat in a disagreement with the existing literature on this topic (Fourty et al.,
673 1996; Jacquemoud et al., 1996; Wang et al., 2015). This outcome can be explained by the new spectral
674 feature selection procedure applied in our study. The results in Figure 5 illustrate why systematically lower
675 performances were reported when attempting to estimate *LMA* and proteins by PROSPECT inversion
676 using a full contiguous spectral information containing spectral regions strongly confounded by water
677 absorption. They also provide the evidence that water absorption does not significantly interfere with the
678 spectral information selected as optimal for retrieval of protein and *CBC* contents in dry but also fresh leaf
679 samples in this study. Therefore, the PROSPECT-PRO protein and *CBC* estimation errors do not originate
680 from the model physical and spectral limitations but from the design of the inversion procedure and from
681 associated criterions of the minimization functions.

682

683 d. Complementarity of chlorophyll and protein estimates as proxies for nitrogen
684 content

685 Despite the known limitations of using chlorophyll *a+b* content as a proxy of N in remote sensing
686 monitoring applications, it has proved to be relatively successful in a certain number of cases (Baret et al.,
687 2007). The main advantage of estimating chlorophyll over protein content is its strong optical signal in the

688 VNIR (especially red-edge) domain, allowing for its accurate RS estimates even at the canopy level (e.g.,
689 Malenovský et al., 2013). In contrast, the SWIR domain, which is required to estimate protein content, but
690 is characterized by lower solar energy flux and lower SNR (Guanter et al., 2015). Therefore, even if being
691 physiologically more robust over a broader range of conditions and vegetation types, the estimation of N
692 from protein content may be associated with a significantly higher uncertainty originating from a weaker
693 SNR of the spectroscopic measurements. The enhanced capacity of PROSPECT-PRO to monitor vegetation
694 C:N ratio and its seasonal changes through the separation of protein and *CBC* contents may prove useful,
695 if systematically and rationally complemented by a RS chlorophyll monitoring.

696

697 e. Potential application for a canopy scale ecosystem nitrogen mapping

698 Physical RT modeling is a key component in revealing the underlying relations between quantitative
699 vegetation properties and information encoded in RS optical data. In this study, we successfully calibrated
700 and validated a new PROSPECT-PRO model that separates nitrogen-based protein constituents from other
701 carbon-based constituents, i.e. cellulose, lignin, hemicellulose, sugars and starch. Unlike previous
702 attempts, which either resulted in a poor protein content estimation performance (Jacquemoud et al.,
703 1996) or suggested a limited accuracy of *LMA* predictions (Wang et al., 2015), the indirect estimation of
704 *LMA* with PROSPECT-PRO (i.e., the sum of protein and *CBC* contents) was found to be fully comparable
705 with the direct estimation of *LMA* using PROSPECT-D. The performances in forward simulations of leaf
706 optical properties were also very similar for both model versions. Similar to Féret et al. (2019), an accurate
707 estimation of *LMA* and its two components required selection of the appropriate spectral domains. The
708 relatively narrow spectral domain identified as optimal for the retrieval of proteins (2100-2139 and 2160-
709 2179 nm) must be considered in the future operational applications for nitrogen or *LMA* monitoring using
710 field and air-/space-borne imaging spectroscopy. This may be incorporated by applying appropriate
711 weights for the different spectral domains that optimize the sensitivity of retrieval algorithms to the

712 constituents of interest. The unsuitable spectral wavelengths can be identified and removed by hybrid
713 band selection methods, feature extraction or band weighting procedures (Fassnacht et al., 2014;
714 Feilhauer et al., 2015; Verrelst et al., 2015).

715 Results of this study offer a new opportunity for operational RS monitoring and consequent management
716 of nitrogen in agricultural and natural ecosystems. However, applicability of PROSPECT-PRO for such a
717 monitoring system is strongly dependent on scalability of the simulated leaf SWIR spectral signatures up
718 to spatially and spectrally heterogeneous canopies. The potential of transferring a PROSPECT-PRO-based
719 N estimating method into an operational application in the field is yet to be investigated. Although
720 proximal remote sensing of small homogeneous canopies, based for instance on the PROCOSINE model
721 (Jay et al., 2016; Morel et al., 2018), could be considered as an intermediate step, a certain number of
722 challenges must be addressed first. These include the capacity to perform sufficiently accurate outdoor
723 canopy measurements, a suppression of the vegetation canopy reflectance angular anisotropy (including
724 spectral effects of background surfaces and leaf orientation), and an ability to achieve a sufficiently high
725 signal-to-noise ratio in the SWIR domain. More generally, analyzing canopy reflectance requires
726 accounting for multiple confounding factors, such as the structural properties of the canopy (i.e., leaf area
727 index, leaf angle distribution and foliage clumping), spectral properties of soil, understory and
728 atmosphere, and the sun-object-observer geometry at the time of data acquisition.

729 Our results indicate the importance of narrow SWIR domains, which will remain to be important also at
730 the canopy level. Current multispectral spaceborne data (e.g., Landsat 8/9 and Sentinel-2 images) do not
731 comply with the narrowband SWIR spectral requirements that we identified, and further investigations
732 are necessary to conclude on feasibility and limitations of its potential use for N mapping using PROSPECT-
733 PRO. An increasing number of available space-borne imaging spectroscopy data (Berger et al., 2020b) is
734 bringing new opportunities in this field. Several satellite platforms are already operational or close to
735 launch, e.g. PRISMA (Loizzo et al., 2019), Gaofen-5 (Liu et al., 2019), or EnMap (Guanter et al., 2015), and

736 few more candidate missions are in preparation, such as the Copernicus Hyperspectral Imaging Mission
737 for the Environment (CHIME) (Nieke and Rast, 2018) or NASA’s EMIT (Green et al., 2019) and Surface
738 Biology and Geology (SBG) missions (Committee on the Decadal Survey for Earth Science and Applications
739 from Space et al., 2018; Hochberg et al., 2015). Data provided by these instruments holds a strong
740 prospect for N monitoring. Yet, preparatory studies will be necessary to analyze the potential of
741 PROSPECT-PRO in simulating sufficiently accurate imaging spectroscopy data of canopies when being
742 coupled with canopy RT models, for instance with SAIL (Berger et al., 2018; Jacquemoud et al., 2009;
743 Verhoef et al., 2007), SCOPE (van der Tol et al., 2009) , INFORM (Schlerf and Atzberger, 2006) or DART
744 (Gastellu-Etchegorry et al., 2017, 2015). Berger et al. (2020a) studied the potential of PROSPECT-PRO
745 coupled with SAIL for the estimation of crop nitrogen based on airborne imaging spectroscopy. They
746 performed a sensitivity analysis identifying the most relevant spectral bands for this task and concluded
747 on the importance of SWIR bands at 2124 and 2234 nm. Their most optimal spectral bands selected in the
748 NIR and the first part of the SWIR spectra suggest that conclusions of this leaf scale study may differ from
749 conclusions at the canopy scale. Accounting for the canopy reflectance confounding factors may need an
750 additional spectral information, coming from different spectral domains than those required at the leaf
751 scale.

752

753 7. CONCLUSIONS

754 This study introduces PROSPECT-PRO, a new version of the PROSPECT leaf RT model, capable of
755 differentiating proteins from other carbon-based constituents as two independent components of *LMA*.
756 The calibration of PROSPECT-PRO was based on the assumption that proteins and *CBC* are the two main
757 spectrally active constituents of the leaf dry matter. We demonstrated that PROSPECT-PRO performs
758 similarly in estimating protein and *CBC* content of both fresh and dry leaves, a marked improvement over

759 previous attempts. Errors computed between measured and simulated leaf optical properties were
760 relatively low for both types of leaves.

761 Our results, based on leaf optical properties with the 1 nm spectral sampling, revealed that the optimal
762 estimation of leaf protein content at the leaf scale is obtained when using two narrow spectral domains
763 between 2100 and 2139 nm, and between 2160 and 2179 nm. The estimation of protein content, assessed
764 by *NRMSE*, was found to be slightly less accurate than the estimation of *CBC* content or total *LMA*.
765 Additionally, the C:N ratio was successfully estimated from the *CBC*:Proteins ratio retrieved by PROSPECT-
766 PRO inversion. Despite these achievements, further investigations, that would be conducted on
767 independent leaf-scale measurements of leaf optical properties, proteins, nitrogen and *LMA*, are still
768 needed. Canopy-scale studies are also required to test the potential of this new model for operational
769 airborne and space-borne applications. The capability of current satellite multispectral instruments (e.g.,
770 Sentinel-2 and Landsat-8/9) to estimate vegetation protein and *CBC* contents needs to be investigated in
771 light of our findings. However, such estimations may remain extremely challenging, considering the coarse
772 resolution and limited number of spectral bands of these instruments in the SWIR region. Spaceborne
773 imaging spectroscopy missions with a higher SWIR spectral sampling may be of the critical importance for
774 a future operational nitrogen-containing protein monitoring of agricultural and natural environments.

775

776 8. ACKNOWLEDGMENTS

777 Authors would like to thank Philip Townsend (University of Wisconsin – Madison), Jochem Verrelst
778 (University of Valencia) and also four anonymous reviewers for their comments and advices improving
779 scientific quality and readability of this manuscript. J.-B. Féret and F. de Boissieu acknowledge financial
780 support from Agence Nationale de la Recherche (BioCop project—ANR-17-CE32-0001) and TOSCA
781 program grant of the French Space Agency (CNES) (HyperTropik/HyperBIO project). Contribution of Z.
782 Malenovský was supported by the Australian Research Council Future Fellowship ‘Bridging Scales in

783 Remote Sensing of Vegetation Stress' (FT160100477). Katja Berger is funded within the EnMAP scientific
784 preparation program under the DLR Space Administration with resources from the German Federal
785 Ministry of Economic Affairs and Energy, grant number 50EE1923. Further, the research was supported
786 by the Action CA17134 SENSECO (Optical synergies for spatiotemporal sensing of scalable
787 ecophysiological traits) funded by COST (European Cooperation in Science and Technology, www.cost.eu).

788

789 9. REFERENCES

- 790 Albornoz, F., 2016. Crop responses to nitrogen overfertilization: A review. *Sci. Hortic.* 205, 79–83.
791 <https://doi.org/10.1016/j.scienta.2016.04.026>
- 792 Allen, W.A., Gausman, H.W., Richardson, A.J., 1970. Mean effective optical constants of cotton leaves. *J.*
793 *Opt. Soc. Am.* 60, 542–547. <https://doi.org/10.1364/JOSA.60.000542>
- 794 Allen, W.A., Gausman, H.W., Richardson, A.J., Thomas, J.R., 1969. Interaction of isotropic light with a
795 compact plant leaf. *J. Opt. Soc. Am.* 59, 1376–1379. <https://doi.org/10.1364/JOSA.59.001376>
- 796 Asner, G.P., Martin, R.E., 2009. Airborne spectranomics: Mapping canopy chemical and taxonomic
797 diversity in tropical forests. *Front. Ecol. Environ.* 7, 269–276. <https://doi.org/10.1890/070152>
- 798 Baret, F., Buis, S., 2008. Estimating Canopy Characteristics from Remote Sensing Observations: Review of
799 Methods and Associated Problems, in: Liang, S. (Ed.), *Advances in Land Remote Sensing*.
800 Springer Netherlands, Dordrecht, pp. 173–201.
- 801 Baret, F., Houles, V., Guerif, M., 2007. Quantification of plant stress using remote sensing observations
802 and crop models: the case of nitrogen management. *J. Exp. Bot.* 58, 869–880.
803 <https://doi.org/10.1093/jxb/erl231>
- 804 Berger, K., Atzberger, C., Danner, M., D'Urso, G., Mauser, W., Vuolo, F., Hank, T., 2018. Evaluation of the
805 PROSAIL Model Capabilities for Future Hyperspectral Model Environments: A Review Study.
806 *Remote Sens.* 10, 85. <https://doi.org/10.3390/rs10010085>
- 807 Berger, K., Verrelst, J., Féret, J.-B., Hank, T., Woche, M., Mauser, W., Camps-Valls, G., 2020a. Retrieval
808 of aboveground crop nitrogen content with a hybrid machine learning method. *Int. J. Appl. Earth*
809 *Obs. Geoinformation* 92, 102174. <https://doi.org/10.1016/j.jag.2020.102174>
- 810 Berger, K., Verrelst, J., Féret, J.-B., Wang, Z., Woche, M., Strathmann, M., Danner, M., Mauser, W.,
811 Hank, T., 2020b. Crop nitrogen monitoring: Recent progress and principal developments in the
812 context of imaging spectroscopy missions. *Remote Sens. Environ.* 242, 111758.
813 <https://doi.org/10.1016/j.rse.2020.111758>
- 814 Borchers, H.W., 2019. *pracma: Practical Numerical Math Functions*.
- 815 Boren, E.J., Boschetti, L., Johnson, D.M., 2019. Characterizing the Variability of the Structure Parameter
816 in the PROSPECT Leaf Optical Properties Model. *Remote Sens.* 11, 1236.
817 <https://doi.org/10.3390/rs11101236>
- 818 Botha, E.J., Zebarth, B.J., Leblon, B., 2006. Non-destructive estimation of potato leaf chlorophyll and
819 protein contents from hyperspectral measurements using the PROSPECT radiative transfer
820 model. *Can. J. Plant Sci.* 86, 279–291. <https://doi.org/10.4141/P05-017>
- 821 Bradstreet, R.B., 1954. Kjeldahl Method for Organic Nitrogen. *Anal. Chem.* 26, 185–187.
822 <https://doi.org/10.1021/ac60085a028>

823 Brown, B., Westcott, M., Christensen, N., Pan, B., Stark, J., 2005. Nitrogen management for hard wheat
824 protein enhancement (No. PNW 578). Washington State Univ. Coop. Ext.

825 Cannavó, F., 2012. Sensitivity analysis for volcanic source modeling quality assessment and model
826 selection. *Comput. Geosci.* 44, 52–59. <https://doi.org/10.1016/j.cageo.2012.03.008>

827 Clevers, J.G., Kooistra, L., 2012. Using hyperspectral remote sensing data for retrieving canopy
828 chlorophyll and nitrogen content. *Sel. Top. Appl. Earth Obs. Remote Sens. IEEE J. Of* 5, 574–583.

829 Clevers, J.G.P.W., Gitelson, A.A., 2013. Remote estimation of crop and grass chlorophyll and nitrogen
830 content using red-edge bands on Sentinel-2 and -3. *Int. J. Appl. Earth Obs. Geoinformation* 23,
831 344–351. <https://doi.org/10.1016/j.jag.2012.10.008>

832 Colombo, R., Meroni, M., Marchesi, A., Busetto, L., Rossini, M., Giardino, C., Panigada, C., 2008.
833 Estimation of leaf and canopy water content in poplar plantations by means of hyperspectral
834 indices and inverse modeling. *Remote Sens. Environ.* 112, 1820–1834.
835 <https://doi.org/10.1016/j.rse.2007.09.005>

836 Committee on the Decadal Survey for Earth Science and Applications from Space, Space Studies Board,
837 Division on Engineering and Physical Sciences, National Academies of Sciences, Engineering, and
838 Medicine, 2018. *Thriving on Our Changing Planet: A Decadal Strategy for Earth Observation from*
839 *Space.* National Academies Press, Washington, D.C. <https://doi.org/10.17226/24938>

840 Curran, P.J., 1989. Remote sensing of foliar chemistry. *Remote Sens. Environ.* 30, 271–278.
841 [https://doi.org/10.1016/0034-4257\(89\)90069-2](https://doi.org/10.1016/0034-4257(89)90069-2)

842 Davidson, E.A., David, M.B., Galloway, J.N., Goodale, C.L., Haeuber, R.A., Harrison, J.A., Howarth, R.W.,
843 Jaynes, D.B., Lowrance, R.R., Thomas, N.B., Peel, J.L., Pinder, R.W., Porter, E., Snyder, C.S.,
844 Townsend, A.R., Ward, M.H., 2011. *Excess Nitrogen in the U.S. Environment: Trends, Risks, and*
845 *Solutions.*

846 Elvidge, C.D., 1990. Visible and near infrared reflectance characteristics of dry plant materials. *Int. J.*
847 *Remote Sens.* 11, 1775–1795. <https://doi.org/10.1080/01431169008955129>

848 Evans, J.R., 1989. Photosynthesis and nitrogen relationships in leaves of C3 plants. *Oecologia* 78, 9–19.
849 <https://doi.org/10.1007/BF00377192>

850 Fassnacht, F.E., Neumann, C., Forster, M., Buddenbaum, H., Ghosh, A., Clasen, A., Joshi, P.K., Koch, B.,
851 2014. Comparison of Feature Reduction Algorithms for Classifying Tree Species With
852 Hyperspectral Data on Three Central European Test Sites. *IEEE J. Sel. Top. Appl. Earth Obs.*
853 *Remote Sens.* 7, 2547–2561. <https://doi.org/10.1109/JSTARS.2014.2329390>

854 Feilhauer, H., Asner, G.P., Martin, R.E., 2015. Multi-method ensemble selection of spectral bands related
855 to leaf biochemistry. *Remote Sens. Environ.* 164, 57–65.
856 <https://doi.org/10.1016/j.rse.2015.03.033>

857 Féret, J.-B., Boissieu, F. de, 2020. prospect: an R package to run the leaf model PROSPECT in forward and
858 inverse mode.

859 Féret, J.-B., François, C., Asner, G.P., Gitelson, A.A., Martin, R.E., Bidet, L.P.R., Ustin, S.L., le Maire, G.,
860 Jacquemoud, S., 2008. PROSPECT-4 and 5: Advances in the leaf optical properties model
861 separating photosynthetic pigments. *Remote Sens. Environ.* 112, 3030–3043.
862 <https://doi.org/10.1016/j.rse.2008.02.012>

863 Féret, J.-B., Gitelson, A.A., Noble, S.D., Jacquemoud, S., 2017. PROSPECT-D: Towards modeling leaf
864 optical properties through a complete lifecycle. *Remote Sens. Environ.* 193, 204–215.
865 <https://doi.org/10.1016/j.rse.2017.03.004>

866 Féret, J.-B., le Maire, G., Jay, S., Berveiller, D., Bendoula, R., Hmimina, G., Cheraïet, A., Oliveira, J.C.,
867 Ponzoni, F.J., Solanki, T., de Boissieu, F., Chave, J., Nouvellon, Y., Porcar-Castell, A., Proisy, C.,
868 Soudani, K., Gastellu-Etchegorry, J.-P., Lefèvre-Fonollosa, M.-J., 2019. Estimating leaf mass per
869 area and equivalent water thickness based on leaf optical properties: Potential and limitations

870 of physical modeling and machine learning. *Remote Sens. Environ.* 231, 110959.
871 <https://doi.org/10.1016/j.rse.2018.11.002>

872 Fletcher, R., 2000. *Practical Methods of Optimization: Fletcher/Practical Methods of Optimization*. John
873 Wiley & Sons, Ltd, Chichester, West Sussex England. <https://doi.org/10.1002/9781118723203>

874 Fourty, Th., Baret, F., Jacquemoud, S., Schmuck, G., Verdebout, J., 1996. Leaf optical properties with
875 explicit description of its biochemical composition: Direct and inverse problems. *Remote Sens.*
876 *Environ.* 56, 104–117. [https://doi.org/10.1016/0034-4257\(95\)00234-0](https://doi.org/10.1016/0034-4257(95)00234-0)

877 Gastellu-Etchegorry, J.-P., Lauret, N., Yin, T., Landier, L., Kallel, A., Malenovský, Z., Bitar, A.A., Aval, J.,
878 Benhmida, S., Qi, J., Medjdoub, G., Guilleux, J., Chavanon, E., Cook, B., Morton, D., Chrysoulakis,
879 N., Mitraka, Z., 2017. DART: Recent Advances in Remote Sensing Data Modeling With
880 Atmosphere, Polarization, and Chlorophyll Fluorescence. *IEEE J. Sel. Top. Appl. Earth Obs.*
881 *Remote Sens.* 10, 2640–2649. <https://doi.org/10.1109/JSTARS.2017.2685528>

882 Gastellu-Etchegorry, J.-P., Yin, T., Lauret, N., Cajgfinger, T., Gregoire, T., Grau, E., Feret, J.-B., Lopes, M.,
883 Guilleux, J., Dedieu, G., Malenovský, Z., Cook, B.D., Morton, D., Rubio, J., Durrieu, S., Cazanave,
884 G., Martin, E., Ristorcelli, T., 2015. Discrete Anisotropic Radiative Transfer (DART 5) for Modeling
885 Airborne and Satellite Spectroradiometer and LIDAR Acquisitions of Natural and Urban
886 Landscapes. *Remote Sens.* 7, 1667–1701. <https://doi.org/10.3390/rs70201667>

887 Green, R., Mahowald, N., Thompson, D., Clark, R., Ehlmann, B., Ginoux, P., Kalashnikova, O., Miller, R.,
888 Okin, G., Painter, T., Perez, C., Realmuto, V., Swayze, G., Middleton, E., Guanter, L., Ben Dor, E.,
889 2019. The Earth Surface Mineral Dust Source Investigation Planned for the International Space
890 Station, in: *Geophysical Research Abstracts*. Presented at the European Geosciences Union,
891 Vienna (Austria).

892 Gruber, N., Galloway, J.N., 2008. An Earth-system perspective of the global nitrogen cycle. *Nature* 451,
893 293–296. <https://doi.org/10.1038/nature06592>

894 Guanter, L., Kaufmann, H., Segl, K., Foerster, S., Rogass, C., Chabrillat, S., Kuester, T., Hollstein, A.,
895 Rossner, G., Chlebek, C., Straif, C., Fischer, S., Schrader, S., Storch, T., Heiden, U., Mueller, A.,
896 Bachmann, M., Mühle, H., Müller, R., Habermeyer, M., Ohndorf, A., Hill, J., Buddenbaum, H.,
897 Hostert, P., van der Linden, S., Leitão, P., Rabe, A., Doerffer, R., Krasemann, H., Xi, H., Mauser,
898 W., Hank, T., Locherer, M., Rast, M., Staenz, K., Sang, B., 2015. The EnMAP Spaceborne Imaging
899 Spectroscopy Mission for Earth Observation. *Remote Sens.* 7, 8830–8857.
900 <https://doi.org/10.3390/rs70708830>

901 Hank, T.B., Berger, K., Bach, H., Clevers, J.G.P.W., Gitelson, A., Zarco-Tejada, P., Mauser, W., 2019.
902 Spaceborne Imaging Spectroscopy for Sustainable Agriculture: Contributions and Challenges.
903 *Surv. Geophys.* 40, 515–551. <https://doi.org/10.1007/s10712-018-9492-0>

904 Himmelsbach, D.S., Boer, H., Akin, D.E., Barton, F.E.I., 1988. Solid-state ¹³C NMR, FTIR, and NIRS
905 spectroscopic studies of ruminant silage digestion, in: *Analytical Applications of Spectroscopy*.
906 Royal Society of Chemistry, London.

907 Hochberg, E.J., Roberts, D.A., Dennison, P.E., Hulley, G.C., 2015. Special issue on the Hyperspectral
908 Infrared Imager (HyspIRI): Emerging science in terrestrial and aquatic ecology, radiation balance
909 and hazards. *Remote Sens. Environ.* 167, 1–5. <https://doi.org/10.1016/j.rse.2015.06.011>

910 Homolova, L., Malenovský, Z., Clevers, J.G., García-Santos, G., Schaepman, M.E., 2013. Review of optical-
911 based remote sensing for plant trait mapping. *Ecol. Complex.* 15, 1–16.

912 Hosgood, B., Jacquemoud, S., Andreoli, G., Verdebout, J., Pedrini, A., Schmuck, G., 1994. Leaf Optical
913 Properties Experiment 93 (LOPEX93) (European Commission No. EUR 16095 EN). Joint Research
914 Centre, Institute for Remote Sensing Applications.

915 Jacquemoud, S., Baret, F., 1990. PROSPECT: A model of leaf optical properties spectra. *Remote Sens.*
916 *Environ.* 34, 75–91. [https://doi.org/10.1016/0034-4257\(90\)90100-Z](https://doi.org/10.1016/0034-4257(90)90100-Z)

- 917 Jacquemoud, S., Ustin, S.L., Verdebout, J., Schmuck, G., Andreoli, G., Hosgood, B., 1996. Estimating leaf
918 biochemistry using the PROSPECT leaf optical properties model. *Remote Sens. Environ.* 56, 194–
919 202. [https://doi.org/10.1016/0034-4257\(95\)00238-3](https://doi.org/10.1016/0034-4257(95)00238-3)
- 920 Jacquemoud, S., Verhoef, W., Baret, F., Bacour, C., Zarco-Tejada, P.J., Asner, G.P., François, C., Ustin, S.L.,
921 2009. PROSPECT+ SAIL models: A review of use for vegetation characterization. *Remote Sens.*
922 *Environ.* 113, S56–S66. <https://doi.org/doi:10.1016/j.rse.2008.01.026>
- 923 Jay, S., Bendoula, R., Hadoux, X., Féret, J.-B., Gorretta, N., 2016. A physically-based model for retrieving
924 foliar biochemistry and leaf orientation using close-range imaging spectroscopy. *Remote Sens.*
925 *Environ.* 177, 220–236. <https://doi.org/10.1016/j.rse.2016.02.029>
- 926 Kant, S., Bi, Y.-M., Rothstein, S.J., 2011. Understanding plant response to nitrogen limitation for the
927 improvement of crop nitrogen use efficiency. *J. Exp. Bot.* 62, 1499–1509.
928 <https://doi.org/10.1093/jxb/erq297>
- 929 Kokaly, R.F., Asner, G.P., Ollinger, S.V., Martin, M.E., Wessman, C.A., 2009. Characterizing canopy
930 biochemistry from imaging spectroscopy and its application to ecosystem studies. *Remote Sens.*
931 *Environ.* 113, S78–S91.
- 932 Kudo, M., Sklansky, J., 2000. Comparison of algorithms that select features for pattern classifiers.
933 *Pattern Recognit.* 33, 25–41. [https://doi.org/10.1016/S0031-3203\(99\)00041-2](https://doi.org/10.1016/S0031-3203(99)00041-2)
- 934 Liu, T., Ren, T., White, P.J., Cong, R., Lu, J., 2018. Storage nitrogen co-ordinates leaf expansion and
935 photosynthetic capacity in winter oilseed rape. *J. Exp. Bot.* 69, 2995–3007.
936 <https://doi.org/10.1093/jxb/ery134>
- 937 Liu, Y.-N., Zhang, J., Zhang, Y., Sun, W.-W., Jiao, L.-L., Sun, D.-X., Hu, X.-N., Ye, X., Li, Y.-D., Liu, S.-F., Cao,
938 K.-Q., Chai, M.-Y., Zhou, W.-Y.-N., 2019. The Advanced Hyperspectral Imager: Aboard China's
939 GaoFen-5 Satellite. *IEEE Geosci. Remote Sens. Mag.* 7, 23–32.
940 <https://doi.org/10.1109/MGRS.2019.2927687>
- 941 Loizzo, R., Daraio, M., Guarini, R., Longo, F., Lorusso, R., Dini, L., Lopinto, E., 2019. Prisma Mission Status
942 and Perspective, in: *IGARSS 2019 - 2019 IEEE International Geoscience and Remote Sensing*
943 *Symposium*. Presented at the *IGARSS 2019 - 2019 IEEE International Geoscience and Remote*
944 *Sensing Symposium*, IEEE, Yokohama, Japan, pp. 4503–4506.
945 <https://doi.org/10.1109/IGARSS.2019.8899272>
- 946 Ma, S., He, F., Tian, D., Zou, D., Yan, Z., Yang, Y., Zhou, T., Huang, K., Shen, H., Fang, J., 2018. Variations
947 and determinants of carbon content in plants: a global synthesis. *Biogeosciences* 15, 693–702.
948 <https://doi.org/10.5194/bg-15-693-2018>
- 949 Malagoli, P., 2005. Dynamics of Nitrogen Uptake and Mobilization in Field-grown Winter Oilseed Rape
950 (*Brassica napus*) from Stem Extension to Harvest: I. Global N Flows between Vegetative and
951 Reproductive Tissues in Relation to Leaf Fall and their Residual N. *Ann. Bot.* 95, 853–861.
952 <https://doi.org/10.1093/aob/mci091>
- 953 Malenovský, Z., Albrechtová, J., Lhotáková, Z., Zurita-Milla, R., Clevers, J.G.P.W., Schaepman, M.E.,
954 Cudlín, P., 2006. Applicability of the PROSPECT model for Norway spruce needles. *Int. J. Remote*
955 *Sens.* 27, 5315–5340. <https://doi.org/10.1080/01431160600762990>
- 956 Malenovský, Z., Homolová, L., Lukeš, P., Buddenbaum, H., Verrelst, J., Alonso, L., Schaepman, M.E.,
957 Lauret, N., Gastellu-Etchegorry, J.-P., 2019. Variability and Uncertainty Challenges in Scaling
958 Imaging Spectroscopy Retrievals and Validations from Leaves Up to Vegetation Canopies. *Surv.*
959 *Geophys.* 40, 631–656. <https://doi.org/10.1007/s10712-019-09534-y>
- 960 Malenovský, Z., Homolová, L., Zurita-Milla, R., Lukeš, P., Kaplan, V., Hanuš, J., Gastellu-Etchegorry, J.-P.,
961 Schaepman, M.E., 2013. Retrieval of spruce leaf chlorophyll content from airborne image data
962 using continuum removal and radiative transfer. *Remote Sens. Environ.* 131, 85–102.
- 963 Marcano-Cedeno, A., Quintanilla-Dominguez, J., Cortina-Januchs, M.G., Andina, D., 2010. Feature
964 selection using Sequential Forward Selection and classification applying Artificial Metaplasticity

965 Neural Network, in: IECON 2010 - 36th Annual Conference on IEEE Industrial Electronics Society.
966 Presented at the IECON 2010 - 36th Annual Conference of IEEE Industrial Electronics, IEEE,
967 Glendale, AZ, USA, pp. 2845–2850. <https://doi.org/10.1109/IECON.2010.5675075>

968 Masclaux-Daubresse, C., Daniel-Vedele, F., Dechorgnat, J., Chardon, F., Gaufichon, L., Suzuki, A., 2010.
969 Nitrogen uptake, assimilation and remobilization in plants: challenges for sustainable and
970 productive agriculture. *Ann. Bot.* 105, 1141–1157. <https://doi.org/10.1093/aob/mcq028>

971 Morel, J., Jay, S., Féret, J.-B., Bakache, A., Bendoula, R., Carreel, F., Gorretta, N., 2018. Exploring the
972 potential of PROCOSINE and close-range hyperspectral imaging to study the effects of fungal
973 diseases on leaf physiology. *Sci. Rep.* 8. <https://doi.org/10.1038/s41598-018-34429-0>

974 Nieke, J., Rast, M., 2018. Towards the Copernicus Hyperspectral Imaging Mission For The Environment
975 (CHIME), in: IGARSS 2018 - 2018 IEEE International Geoscience and Remote Sensing Symposium.
976 Presented at the IGARSS 2018 - 2018 IEEE International Geoscience and Remote Sensing
977 Symposium, IEEE, Valencia, pp. 157–159. <https://doi.org/10.1109/IGARSS.2018.8518384>

978 Paul, M.J., Driscoll, S.P., 1997. Sugar repression of photosynthesis: the role of carbohydrates in signalling
979 nitrogen deficiency through source:sink imbalance. *Plant Cell Environ.* 20, 110–116.
980 <https://doi.org/10.1046/j.1365-3040.1997.d01-17.x>

981 Pedrós, R., Goulas, Y., Jacquemoud, S., Louis, J., Moya, I., 2010. FluorMODleaf: A new leaf fluorescence
982 emission model based on the PROSPECT model. *Remote Sens. Environ.* 114, 155–167.

983 Reich, P.B., Hobbie, S.E., Lee, T., Ellsworth, D.S., West, J.B., Tilman, D., Knops, J.M.H., Naeem, S., Trost, J.,
984 2006. Nitrogen limitation constrains sustainability of ecosystem response to CO₂. *Nature* 440,
985 922–925. <https://doi.org/10.1038/nature04486>

986 Sáez-Plaza, P., Michałowski, T., Navas, M.J., Asuero, A.G., Wybraniec, S., 2013. An Overview of the
987 Kjeldahl Method of Nitrogen Determination. Part I. Early History, Chemistry of the Procedure,
988 and Titrimetric Finish. *Crit. Rev. Anal. Chem.* 43, 178–223.
989 <https://doi.org/10.1080/10408347.2012.751786>

990 Schaepman-Strub, G., Schaepman, M.E., Painter, T.H., Dangel, S., Martonchik, J.V., 2006. Reflectance
991 quantities in optical remote sensing—definitions and case studies. *Remote Sens. Environ.* 103,
992 27–42. <https://doi.org/10.1016/j.rse.2006.03.002>

993 Schlerf, M., Atzberger, C., 2006. Inversion of a forest reflectance model to estimate structural canopy
994 variables from hyperspectral remote sensing data. *Remote Sens. Environ.* 100, 281–294.
995 <https://doi.org/10.1016/j.rse.2005.10.006>

996 Serbin, S.P., Wu, J., Ely, K.S., Kruger, E.L., Townsend, P.A., Meng, R., Wolfe, B.T., Chlus, A., Wang, Z.,
997 Rogers, A., 2019. From the Arctic to the tropics: multibiome prediction of leaf mass per area
998 using leaf reflectance. *New Phytol.* 224, 1557–1568. <https://doi.org/10.1111/nph.16123>

999 Sharwood, R.E., 2017. Engineering chloroplasts to improve Rubisco catalysis: prospects for translating
1000 improvements into food and fiber crops. *New Phytol.* 213, 494–510.
1001 <https://doi.org/10.1111/nph.14351>

1002 Ustin, S.L., Jacquemoud, S., 2020. How the Optical Properties of Leaves Modify the Absorption and
1003 Scattering of Energy and Enhance Leaf Functionality, in: Cavender-Bares, J., Gamon, J.A.,
1004 Townsend, P.A. (Eds.), *Remote Sensing of Plant Biodiversity*. Springer International Publishing,
1005 Cham, pp. 349–384. https://doi.org/10.1007/978-3-030-33157-3_14

1006 van der Tol, C., Verhoef, W., Timmermans, J., Verhoef, A., Su, Z., 2009. An integrated model of soil-
1007 canopy spectral radiances, photosynthesis, fluorescence, temperature and energy balance.
1008 *Biogeosciences* 6, 3109–3129. <https://doi.org/10.5194/bg-6-3109-2009>

1009 van der Tol, C., Vilfan, N., Dauwe, D., Cendrero-Mateo, M.P., Yang, P., 2019. The scattering and re-
1010 absorption of red and near-infrared chlorophyll fluorescence in the models Fluspect and SCOPE.
1011 *Remote Sens. Environ.* 232, 111292. <https://doi.org/10.1016/j.rse.2019.111292>

1012 Verdebout, J., Jacquemoud, S., Andreoli, G., Hosgood, B., Pedrini, A., Schmuck, G., 1995. Analysis of
1013 imaging spectrometer data to evaluate the biochemical content of vegetation, based on the
1014 results of a laboratory experiment, in: Mougin, E., Ranson, K.J., Smith, J.A. (Eds.), . Presented at
1015 the Satellite Remote Sensing, Rome, Italy, pp. 63–76. <https://doi.org/10.1117/12.200746>
1016 Verhoef, W., Jia, L., Xiao, Q., Su, Z., 2007. Unified optical-thermal four-stream radiative transfer theory
1017 for homogeneous vegetation canopies. *IEEE Trans. Geosci. Remote Sens.* 45, 1808–1822.
1018 <https://doi.org/10.1109/TGRS.2007.895844>
1019 Verrelst, J., Camps-Valls, G., Muñoz-Marí, J., Rivera, J.P., Veroustraete, F., Clevers, J.G.P.W., Moreno, J.,
1020 2015. Optical remote sensing and the retrieval of terrestrial vegetation bio-geophysical
1021 properties – A review. *ISPRS J. Photogramm. Remote Sens.* 108, 273–290.
1022 <https://doi.org/10.1016/j.isprsjprs.2015.05.005>
1023 Verrelst, J., Malenovský, Z., Van der Tol, C., Camps-Valls, G., Gastellu-Etchegorry, J.-P., Lewis, P., North,
1024 P., Moreno, J., 2019a. Quantifying Vegetation Biophysical Variables from Imaging Spectroscopy
1025 Data: A Review on Retrieval Methods. *Surv. Geophys.* 40, 589–629.
1026 <https://doi.org/10.1007/s10712-018-9478-y>
1027 Verrelst, J., Vicent, J., Rivera-Caicedo, J.P., Lumbierres, M., Morcillo-Pallarés, P., Moreno, J., 2019b.
1028 Global Sensitivity Analysis of Leaf-Canopy-Atmosphere RTMs: Implications for Biophysical
1029 Variables Retrieval from Top-of-Atmosphere Radiance Data. *Remote Sens.* 11, 1923.
1030 <https://doi.org/10.3390/rs11161923>
1031 Vilfan, N., Van der Tol, C., Yang, P., Wyber, R., Malenovský, Z., Robinson, S.A., Verhoef, W., 2018.
1032 Extending Fluspect to simulate xanthophyll driven leaf reflectance dynamics. *Remote Sens.*
1033 *Environ.* 211, 345–356. <https://doi.org/10.1016/j.rse.2018.04.012>
1034 Vitousek, P.M., Aber, J.D., Howarth, R.W., Likens, G.E., Matson, P.A., Schindler, D.W., Schlesinger, W.H.,
1035 Tilman, D.G., 1997. HUMAN ALTERATION OF THE GLOBAL NITROGEN CYCLE: SOURCES AND
1036 CONSEQUENCES. *Ecol. Appl.* 7, 737–750. [https://doi.org/10.1890/1051-](https://doi.org/10.1890/1051-0761(1997)007[0737:HAOTGN]2.0.CO;2)
1037 [0761\(1997\)007\[0737:HAOTGN\]2.0.CO;2](https://doi.org/10.1890/1051-0761(1997)007[0737:HAOTGN]2.0.CO;2)
1038 Vos, J., Bom, M., 1993. Hand-held chlorophyll meter: a promising tool to assess the nitrogen status of
1039 potato foliage. *Potato Res.* 36, 301–308. <https://doi.org/10.1007/BF02361796>
1040 Wang, Z., Skidmore, A.K., Wang, T., Darvishzadeh, R., Hearne, J., 2015. Applicability of the PROSPECT
1041 model for estimating protein and cellulose+lignin in fresh leaves. *Remote Sens. Environ.* 168,
1042 205–218. <https://doi.org/10.1016/j.rse.2015.07.007>
1043 Willmott, C.J., Ackleson, S.G., Davis, R.E., Feddema, J.J., Klink, K.M., Legates, D.R., O'Donnell, J., Rowe,
1044 C.M., 1985. Statistics for the evaluation and comparison of models. *J. Geophys. Res.* 90, 8995.
1045 <https://doi.org/10.1029/JC090iC05p08995>
1046 Wingler, A., Purdy, S., MacLean, J.A., Pourtau, N., 2006. The role of sugars in integrating environmental
1047 signals during the regulation of leaf senescence. *J. Exp. Bot.* 57, 391–399.
1048 <https://doi.org/10.1093/jxb/eri279>
1049 Yeoh, H.-H., Wee, Y.-C., 1994. Leaf protein contents and nitrogen-to-protein conversion factors for 90
1050 plant species. *Food Chem.* 49, 245–250. [https://doi.org/10.1016/0308-8146\(94\)90167-8](https://doi.org/10.1016/0308-8146(94)90167-8)
1051 Yoder, B.J., Pettigrew-Crosby, R.E., 1995. Predicting nitrogen and chlorophyll content and concentrations
1052 from reflectance spectra (400–2500 nm) at leaf and canopy scales. *Remote Sens. Environ.* 53,
1053 199–211. [https://doi.org/10.1016/0034-4257\(95\)00135-N](https://doi.org/10.1016/0034-4257(95)00135-N)
1054 Zheng, Z.-L., 2009. Carbon and nitrogen nutrient balance signaling in plants. *Plant Signal. Behav.* 4, 584–
1055 591. <https://doi.org/10.4161/psb.4.7.8540>
1056 Zhou, G., Xu, S., Ciais, P., Manzoni, S., Fang, J., Yu, G., Tang, X., Zhou, P., Wang, W., Yan, J., Wang, G., Ma,
1057 K., Li, S., Du, S., Han, S., Ma, Y., Zhang, D., Liu, J., Liu, S., Chu, G., Zhang, Q., Li, Y., Huang, W., Ren,
1058 H., Lu, X., Chen, X., 2019. Climate and litter C/N ratio constrain soil organic carbon accumulation.
1059 *Natl. Sci. Rev.* 6, 746–757. <https://doi.org/10.1093/nsr/nwz045>

